Quantum interferences revealed by neutron diffraction accord with a macroscopic-scale quantum-theory of ferroelectrics KH 2(1−ρ) D 2ρ PO 4

François Fillaux, Alain Cousson

EPJ manuscript No.
(will be inserted by the editor)

Quantum interferences revealed by neutron diffraction accord with a macroscopic-scale quantum-theory of ferroelectrics $KH_{2(1-\rho)}D_{2\rho}PO_4$

François Fillaux[1] and Alain Cousson[2]

[1] Sorbonne Universités, UPMC Univ Paris 06, UMR 8233, MONARIS, F-7505 Paris, France
[2] Laboratoire Léon Brillouin (CEA-CNRS), C.E. Saclay, 91191 Gif-sur-Yvette, cedex, France

January 25, 2016

Abstract. Neutron diffraction by single-crystals $KH_{2(1-\rho)}D_{2\rho}PO_4$ at 293 K reveal quantum interferences consistent with a static lattice of entangled proton-deuteron scatterers. These crystals are represented by a macroscopic-scale condensate of phonons with continuous space-time-translation symmetry and zero-entropy. This state is energetically favored and decoherence-free over a wide temperature-range. Projection of the crystal state onto a basis of four electrically- and isotopically-distinct state-vectors accounts for isotope and pressure effects on the temperature of the ferroelectric-dielectric transition, as well as for the latent heat. At the microscopic level, an incoming wave realizes a transitory state either in the space of static positional parameters (elastic scattering) or in that of the symmetry species (energy transfer). Neutron diffraction, vibrational spectroscopy, relaxometry and neutron Compton scattering support the conclusion that proton and deuteron scatterers are separable exclusively through resonant energy-transfer.

PACS. PACS-61.05.F- Neutron diffraction and scattering – PACS-64.70.Tg Quantum phase transition

1 Introduction

The crystal of potassium dihydrogen phosphate (KH_2PO_4 or KDP) belongs to the family of hydrogen-bonded ferroelectrics. Since the discovery of the phase transition showing permanent electric polarization below $T_0 \approx 122$ K [1], there is a continuing interest in understanding the origin of the ferroelectricity, the order of the phase transition, the nature of the symmetry breaking involved, the increase of T_0 and latent heat with the deuteration degree of mixed crystals $KH_{2(1-\rho)}D_{2\rho}PO_4$, or the decrease of T_0 at high pressure. Theoretical models so far published are mostly phenomenological in nature. Apart from technological interests for quantum electronics and nonlinear optics, which are beyond the scope of this present paper, our motivation is to improve our understanding of phase transitions in the field of solid-state physics and solid-state chemistry, via a new theoretical framework based on ground-breaking neutron-diffraction measurements which suggest a macroscopic-scale quantum-state. This theory takes into account the well-established experimental facts listed below.

Crystals $KH_{2(1-\rho)}D_{2\rho}PO_4$ demonstrate three structural phases: the orthorhombic ferroelectric-phase below T_0; the nonpolar tetragonal-phase at intermediate temperatures and the monoclinic variety above T_{cM} [2–11]. Calorimetric studies evidence the first-order character of the ferroelectric transition. T_0 increases linearly with ρ from ≈ 122 K to ≈ 224 K for $\rho \approx 0.98$ [7], while the latent heat increases from ≈ 46 J mol^{-1} [4] to ≈ 440 J mol^{-1} [3]. Below T_0, the electric polarization demonstrates hysteresis loops distinctive of ferroelectricity [7]. Hysteresis vanishes above T_0 and the polarization proportional to the applied electric field suggests a dielectric, rather than paraelectric, phase. On the other hand, $T_{cM}(\rho)$ decreases from ≈ 463 K for KH_2PO_4 to below room temperature for $\rho > 0.8$ [9], but this transition is poorly documented. It is not tackled in this present work.

Orthorhombic and tetragonal KH_2PO_4 ($Z = 2$) are comprised of similar three dimensional networks of indistinguishable PO_4 entities linked through equivalent hydrogen bonds parallel to (a, b) planes [12–26]. Below T_0, each PO_4 with T_d-symmetry is covalently bound to two protons in $H_2PO_4^-$ groupings with C_2-symmetry. Each entity is engaged in four hydrogen bonds with its neighbors. The polarization vector along the c axis is perpendicular to the network of hydrogen bonds. Above T_0, each S_4-PO_4 shares four protons with its neighbors and two sites equidistant from the O···O bond center are equally occupied. Positional parameters of heavy nuclei are similar for the two phases. The decrease of T_0 at high pressure has been tentatively correlated with a decrease of O···O bond lengths (R_{OO}), while the increase of T_0 upon deuteration was as-

Send offprint requests to: francois.fillaux@upmc.fr

cribed to the greater inter-site distances $r_D > r_H$. These correlations are termed "geometric effects".

In contrast with the diffraction pattern, Raman spectra are practically unchanged across T_0. The symmetry-related selection-rules for T_d-PO_4 at C_2 sites and the energy levels for H or D oscillators are virtually unaffected [27–31]. Only a central peak at zero-frequency is markedly impacted by the transition. This peak was tentatively regarded as a soft "ferroelectric-mode" of a displacive transition driven by collective proton-tunneling coupled with heavy atoms [32–34]. However, subsequent studies of the spectral profile suggest a symmetrical quasi-elastic peak instead of the asymmetrical profile of a soft-mode [35–37]. This new interpretation accords with the single-exponential decay on the $10^{-11}s$ time-scale of the signal induced by stimulated Raman [38]. On the other hand, inelastic neutron-scattering (INS) reveals differences between the two phases, which are not yet clearly understood [39,40], and neutron Compton scattering (NCS) highlights changes of the kinetic-momentum for protons and deuterons across T_0 [41,42].

From theory viewpoint, various phenomenological models have been reported. A one-to-one correspondence between the orientation of PO_4 dipole-moments and hydrogen-bond configurations, namely $O_1{-}H\cdots O_2$ or $O_1\cdots H{-}O_2$, or likewise for deuterons, is widely hypothesized. The phase transition, supposedly of the order-disorder type, is ascribed to a balance of the ordering tendency of dipolar interactions and the disordering tendency of the temperature [43–47]. Isotope effects are supposed to arise from hypothetical double-well potentials along $O\cdots O$ coordinates, either asymmetrical below T_0 or symmetrical above T_0, so that the disordering tendency of tunnelling counterbalances the ordering tendency of dipolar interactions more efficiently for protons than for deuterons [48–50]. In order to account for isotope and pressure effects, a dividing R_{OO}-value has been suggested, between symmetrical double-wells for shorter bonds and asymmetrical double-wells for longer bonds [51–57]. Alternatively, displacive models supposing a ferroelectric-mode [58,59], or PO_4 distortions [60–64], were reported. So far, computational methods have not pinpointed any key parameter [65–71].

Every theoretical model we are aware of is actually somehow in conflict, or in tension, with observations. a) Nelmes [24] has continuously insisted that there is no crystallographic evidence of statistical disorder above T_0, neither for H in KH_2PO_4, nor for D in $KH_{2(1-\rho)}D_{2\rho}PO_4$ ($\rho = 0.95$). b) In contrast with Slater's hypothesis [43], the polarization should not depend on proton or deuteron displacements across bonds parallel to the basal planes, which are perpendicular to the electric field, so the supposed ordering tendency of dipolar interactions is questionable. c) In contrast with Blinc's model [48], symmetric double-wells are forbidden by the lack of symmetry-planes perpendicular to $O\cdots O$ bonds. d) The soft-mode scheme [58] is questioned by advanced Raman studies. e) None of the reported models accounts for isotope effects on the latent heat [3,4]. With hindsight, the great variety of models so far investigated suggests that there is little chance of success, if any, in pursuing the same lines of reasoning.

We are, therefore, encouraged to envisage a radically new framework inspired by spatially-extended quantum effects, excluding disorder, reported for nonferroic crystals of bicarbonate $KH_{(1-\rho)}D_\rho CO_3$ [72–80]. In particular, it was shown that asymmetric double-well operators for proton stretching account for a quasi-elastic peak similar to that reported for KH_2PO_4. Conversely, we tentatively infer that the central peak of KDP could be an evidence to suggest double-wells and macroscopic-scale quantum effects. However, previous diffraction works left open to question whether or not isotope disorder can be effectively ruled out for any ρ-value. In Sect. 2 we show that for $\rho \approx 0.51$ and 0.65, single-crystal neutron-diffraction gives no evidence for statistical disorder at room temperature, quite in line with Nelmes' conclusions. In addition, thermal functions reveal quantum interferences suggesting nonseparable proton and deuteron scatterers. To the best of our knowledge, this is unprecedented. The theory presented in Sect. 3 is based on these foundational outcomes.

2 Neutron diffraction

Single crystals $KH_{2(1-\rho)}D_{2\rho}PO_4$, $\rho = 0.00, 0.51, 0.65$, were grown from saturated solutions in H_2O/D_2O mixtures. Specimens $\approx 3\times3\times3$ mm^3 at (293 ± 1) K were measured with the four-circle diffractometer 5C2 based at the Orphée reactor of the Laboratoire Léon-Brillouin [81]. Data reduction and analysis were carried out with CRYSTALS [82] (see supplemental files KH2PO4.cif, KH-0.49-D-0.51-PO4.cif and KH-0.35-D-0.65-PO4.cif) [83].

Inspection of intensities for absent reflections confirms the tetragonal $I\bar{4}2d$ (D_{2d}^{12}) space group assignment ($Z = 2$) for every ρ-value. There is no visible symmetry breaking to suggest a random distribution of mutually exclusive H- and D-nuclei. During the refinement procedure, positional and thermal parameters, as well as occupancy factors at proton and deuteron sites (p_H, p_D), were allowed to converge freely. The best parameters gathered in supplemental Tables [84] accord with those reported in a previous work [23]. $R_{OO}(\rho) = (1-\rho)R_{OHO} + \rho R_{ODO}$, where $R_{OHO} \approx 2.48$ Å and $R_{ODO} \approx 2.52$ Å, suggests a linear combination of KH_2PO_4 and KD_2PO_4 sublattices, in accordance with Raman [30]. The PO_4 geometry is practically ρ-independent.

The freely refined occupancy factors are such that $p_H(\rho)+p_D(\rho) = 1.00(1)$. There is no visible loss of coherent-scattering intensity due to disorder. Let $\bar{b}_H = -3.741$ fm and $\bar{b}_D = 6.671$ fm be the coherent scattering lengths. The coherent cross-section for a random distribution of mutually exclusive nuclei is $\sigma_c(\rho) = 4\pi[(1-\rho)\bar{b}_H+\rho\bar{b}_D]^2$. This is less than $4\pi[(1-\rho)\bar{b}_H^2+\rho\bar{b}_D^2]$ for distinct disorder-free sublattices of protons and deuterons [85,86]. The difference is the incoherent cross-section induced by isotope disorder, viz $\sigma_i(\rho) = 4\pi\rho(1-\rho)(\bar{b}_H - \bar{b}_D)^2$, that is a maximum for $\rho = 0.50$, in which case $p_H + p_D = 0.5$. A random distribution of mutually exclusive scatterers is, therefore, ruled out. Diffraction patterns are consistent

with a combination of KH_2PO_4 and KD_2PO_4 sublattices, such that probability densities for protons or deuterons be extended throughout their respective sublattices. These scatterers should be represented by waves instead of localized particle-like entities.

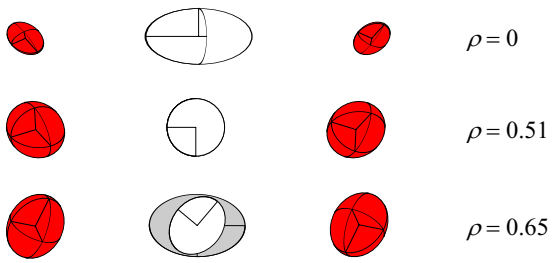

Fig. 1. Projection on (a, b) planes of the 50%-probability thermal functions for $OH_{(1-\rho)}D_\rho O$ at 293 K computed with CRYSTALS [82]. Oxygen is red, Hydrogen is white, Deuterium is grey.

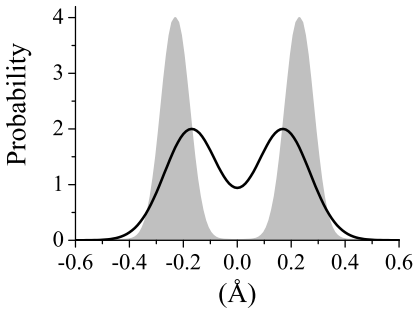

Fig. 2. Modelling nuclear probability densities. Solid: $\psi_H^2 = 2\{\exp[-(x-0.17)^2/0.02]+\exp[-(x+0.17)^2/0.02]\}$. Grey: $\psi_D^2 = 4\{\exp[-(x-0.23)^2/0.005]+\exp[-(x+0.23)^2/0.005]\}$.

In addition, projections of the thermal functions (TF) on (a, b) planes (fig. 1) suggest quantum interferences due to entangled H-D scatterers. In the case $\rho = 0$, the ellipsoid is consistent with two unresolved off-center Gaussian distributions along O···O (fig. 2) and a single Gaussian perpendicular to O···O. For $\rho = 0.51$, the probability density for protons, say H-TF, is nearly isotropic and the deuteron part (D-TF) is invisible. This is at variance with the cross-section ratio for uncorrelated scatterers, viz $\rho\bar{b}_D^2/(1-\rho)\bar{b}_H^2 \approx 4$, that is largely in favour of D-TF. For $\rho = 0.65$, the H-TF is still nearly isotropic and the D-TF appears as crescents on either side of the H-TF.

In order to be more specific, probability densities along O···O bonds can be represented by Gaussian functions centred at ±0.17 Å for H, or ±0.23 Å for D [15,19,20], with variances $\langle u_H^2\rangle \approx 0.02$ Å^2 or $\langle u_D^2\rangle \approx 0.005$ Å^2 (fig. 2). Then, the thermal function for uncorrelated scatterers should be

$$TF_1(\rho) = [(1-\rho)(\bar{b}_H\psi_{H\parallel})^2+\rho(\bar{b}_D\psi_{D\parallel})^2]\exp(-x^2/U), \quad (1)$$

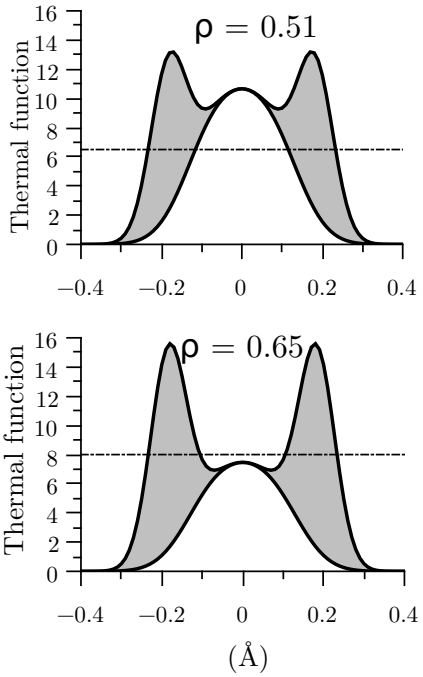

Fig. 3. Modelling the thermal function of $H_{(1-\rho)}D_\rho$ for separable scatterers (1). White for protons, grey for deuterons. Dot dash: 50% of the density at maximum.

where $U \approx 0.02$ Å^2 [84]. For $\rho = 0.51$, the expected deuteron-density is dominant in fig. 3, while it is not observed in fig. 1, and the narrowing of the proton-density observed in fig. 1 is not reproduced in fig. 3.

Alternatively, the thermal function for entangled scatterers reads

$$TF_2(\rho) = [a_H b_H\psi_{H\parallel} + a_D b_D\psi_{D\parallel}]^2\exp(-x^2/U), \quad (2)$$

where $|a_H|^2 = 1-\rho$, $|a_D|^2 = \rho$, a_H/a_D real. In fig. 4, the nodes of density are due to interferences in the range where $\psi_{H\parallel}$ and $\psi_{D\parallel}$ overlap. For $\rho = 0.51$, such interferences account for the narrowing of the proton-density parallel to O···O and for the missing deuteron-density in fig. 1. In that case, $D - TF_2$ is ≈ 20% of $H - TF_2$ (fig. 4), that is below the 50% threshold in fig. 1. For $\rho = 0.65$, similar densities at maximum for protons or deuterons in fig. 4 compare favorably with fig. 1.

Quantum interferences follow from the different locations of proton and deuteron sites along O···O. They are not visible perpendicular to O···O because $\psi_{H\perp}$ and $\psi_{D\perp}$ are single-peaks centred at the same position. In that case, (2) rewritten with the $\psi_\perp$'s yields a sum of indiscernible Gaussian profiles. For $\rho = 0.65$, the crescent-shaped D-TF is consistent with projections of thermal functions parallel or perpendicular onto any direction ϑ with respect to O···O in the basal plane: $\cos\vartheta D-TF_{2\parallel}+\sin\vartheta D-TF_{2\perp}$.

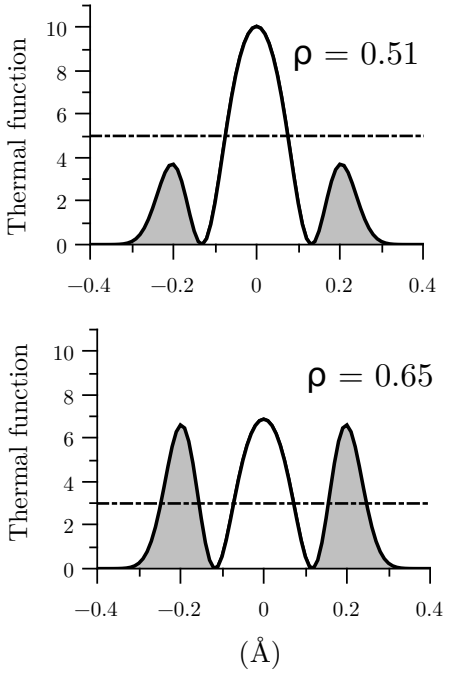

Fig. 4. Modelling the thermal function of $H_{(1-\rho)}D_\rho$ for nonseparable scatterers (2). White for protons, grey for deuterons. Dot dash: 50% of the density at maximum.

In conclusion of this present Sect. 2, neutron diffraction excludes statistical disorder and suggests with reasonable confidence entangled proton-deuteron scatterers. Owing to the different masses, this makes sense if—and only if—the wavefunction is time-independent (time-translation symmetry). On this basis, we propose in Sect. 3 a theory for mixed isotope crystals.

3 Theory

A crystal is commonly represented by a statistical ensemble of nuclear oscillators for which quantum correlations are destroyed by some mechanisms extrinsic to the quantum theory, such as environment-induced decoherence [87–89]. In the harmonic approximation the molar Helmholtz energy for N degrees-of-freedom is:

$$\left.\begin{aligned} A_i &= K + V - TS; \\ &= \sum_{l=1}^{N} \left[\mathcal{N}_0 \frac{h\nu_l}{2} + \mathcal{R}T \ln\left(1 - \exp - \frac{h\nu_l}{kT}\right)\right]; \end{aligned}\right\} \quad (3)$$

where K, V, S, and $\mathcal{N}_0$ are kinetic energy, potential energy, entropy and Avogadro's constant, respectively.

As an alternative to the decoherence scheme, it follows from the linear formalism of quantum mechanics that for each degree of freedom superposition of $\mathcal{N}_0$ phonons $\propto \sum_{n=1}^{\mathcal{N}_0} \exp i(\mathbf{k}.\mathbf{u} - \omega(\mathbf{k})t + \phi_n)$ with an even distribution of phases is a pure state, that complies with the space-group symmetry operator of the crystal. The wavefunction is a constant with continuous space-time-translation symmetry. Wavevectors, relative nuclear positions, phonon states and time are indefinite. The entropy vanishes. The complexity of the statistical representation is hidden and new properties emerge. The eigenenergy for $N\mathcal{N}_0$ free degrees-of-freedom at thermal equilibrium is $N\mathcal{R}\mathcal{T}/2$. It is unique. The "eigentemperature" $\mathcal{T}$ is different in nature from the thermodynamic temperature of the environment T. (In Sects. 3.3 and 3.4 it will appear that $\mathcal{T} = T$ for the ferroelectric phase, while $\mathcal{T} = T - T_0$ for the nonpolar phase.) Such a condensate is stable if $N\mathcal{R}\mathcal{T}/2 < A_i$. Since this condition is satisfied as $TS \longrightarrow 0$ and not satisfied as $TS \longrightarrow \infty$, there is a divide for each mode. We suppose equipartition excludes coexistence of coherent and incoherent subsystems in the same crystal, so the transition temperature of the crystal, say $\mathcal{T}_{ci}$, should depend on the mean oscillator-energy $h\bar{\nu}$. Below $\mathcal{T}_{ci}$, a condensate represents a macroscopically-quantum solid with distinctive symmetry inside which space and time are indefinite [90].

At the microscopic level, an incoming plane-wave (photon or neutron) may break the continuous translation-symmetry and realize a transitory Bloch-state at $\mathcal{T}$, in-phase with the wave, that is not an eigenstate of the crystal. Every single realization yields the same state that can be projected onto the eigenstates of an operator depending on the measurement in question. For instance, diffraction via elastic momentum-transfer breaking the space-translation symmetry yields positional-parameters and thermal functions for static nuclear-densities, which are Fourier transform of the lattice state realized in the momentum representation, while energy levels and time remain indefinite. Alternatively, energy transfer breaking the time-translation symmetry realizes either an eigenstate of the potential operator through resonance (Sect. 3.1) or a superposition through off resonance (Sects. 3.4 and 3.5), while nuclear positions remain indefinite. On the molar-scale, the condensate as a whole is virtually unaffected by a single realization and spontaneous decay (Sect. 3.4) suppresses quantum correlations with the outgoing wave and hence decoherence. In addition, the probability for a wave to entangle a state previously realized is insignificant, so the outcome is independent of previous measurements.

Equation (3) yields $\mathcal{T}_{ci} > 300$ K if $h\bar{\nu} > 350$ cm^{-1}, what is likely for KDP. Consequently, a monodomain crystal $KH_{2(1-\rho)}D_{2\rho}PO_4$ at thermal equilibrium can be tentatively represented by a condensate. In this context, diffraction (Sect. 2) shows that elastic scattering realizes a time-independent lattice-state of nonseparable proton-deuteron scatterers. Alternatively, vibrational spectra analysed below in Sect. 3.1 reveal eigenstates consistent with double-well operators. Then, we show that the transition temperature (Sect. 3.2), the latent heat (Sect. 3.3), the relaxation rate (Sect. 3.4), NCS data (Sect. 3.5) can be rationalized within the condensate framework and conflicts of interpretation are ruled out.

3.1 Double-well operators

Let the static positional-parameters along O···O bond directions of particle-like protons or deuterons in the lattice of unit-cells ($Z = 2$) indexed l ($1 \leq l \leq \mathcal{N}_0/2$) be orthogonal coordinates $x_i = x_{il}$ $\forall l$, $i = 1 \cdots 4$, in the 4-D space $\{x_i\}$. Let the symmetry species for indistinguishable degrees-of-freedom indexed m, $1 \leq m \leq \mathcal{N}_0/2$, be orthogonal coordinates $\chi_j = \chi_{jm}$ $\forall m$, $j = 1 \cdots 4$, in the 4-D space $\{\chi_j\}$. The dispersion-free eigenstates of the potential operators $\mathbb{V}_j(\chi_j)$ are $|\psi_{jn}(\chi_j)\rangle$. $\{x_i\}$ and $\{\chi_j\}$ are subspaces of N-D $\{x\}$ and $\{\chi\}$, respectively.

In classical mechanics, symmetry coordinates for coupled harmonic-oscillators are linear combinations of the nuclear coordinates X_i's, referred to as normal coordinates X_j's (see [91,92] for KH_2PO_4), for which only the ratio of the effective mass to the amplitude is meaningful. X_i's and X_j's belong to one and the same space $\{X\}$ and the causal relationship between nuclear positions and potential energy is a cornerstone of computational models. For example, the Born-Oppenheimer energy-surface computed at fixed nuclear coordinates in X-space and the kinetic energy comprised of partial derivatives with respect to the X_i's yield a classical, time-independent, Hamiltonian for particles with strictly defined positions and momenta, outside the bounds of the uncertainty principle. The eigenstates of this Hamiltonian are different in nature from those revealed by vibrational spectroscopy for quantum nuclei.

Within the condensate framework, any realization pertains either to the wave-like representation, for which the x_i's are indefinite, or to the static particle-like representation, for which the $|\psi_{jn}(\chi_j)\rangle$'s are indefinite. In other words, vibrational states with symmetry-conserving time evolution are confined to the χ-space while symmetry-breaking static configurations in x-space are excluded. The space-time averaged symmetry permitted by classical mechanics is ruled out by quantum mechanics. $\{x_i\}$ and $\{\chi_j\}$ are orthogonal to each other. The χ's are not linear combinations of the x_i's. The $\psi_{jn}(\chi_j)$'s have no counterpart in $\{x_i\}$. There is no causal relationship between nuclear positions and the $\mathbb{V}_j(\chi_j)$'s, which are outside the bounds of computational models in direct space. Vibrational spectroscopy is the only information in hand and we show in Appendix A that the $\mathbb{V}_j(\chi_j)$'s of the ferroelectric KH_2PO_4 are identical asymmetric double-wells for all χ_j's (Table 1), to within spectroscopic resolution.

Let $\mathbb{V}_{j+}(\chi_j)$ and $\mathbb{V}_{j-}(\chi_j)$ be operators with identical energy levels and opposite linear asymmetry (fig. 5). $\mathbb{V}_{\Uparrow} = \bigoplus_j \mathbb{V}_{j+}(\chi_j)$ and $\mathbb{V}_{\Downarrow} = \bigoplus_j \mathbb{V}_{j-}(\chi_j)$ are operators for polarizations either parallel to c ($\Uparrow$, L_j-wells preferred), or antiparallel ($\Downarrow$, R_j-wells preferred). For the ferroelectric crystal, $\mathbb{V}_{\Downarrow} = \mathbb{V}_{\Uparrow} + V_0$, where V_0 is the energy-cost per KH_2PO_4 formula for a polarization-flip with respect to a fixed orientation of the orthorhombic frame. For the tetragonal phase, $V_0 = 0$. In that case, if $\mathbb{V}_{j+}(\chi_j)$ and $\mathbb{V}_{j-}(\chi_j)$ were separable, their energy levels should be degenerate, as shown in fig. 5. By contrast, a rather intense INS band observed at $h\nu_{0\pm} = (10 \pm 2)$ meV/(80 ± 16) cm^{-1} for the tetragonal KH_2PO_4 at $T = 30$ K and 2 GPa [40], that is not observed for the ferroelectric analogue, can be tentatively assigned to the resonance splitting $2^{-1/2}[|0_{\Uparrow j}\rangle \pm |0_{\Downarrow j}\rangle]$ due to overlap of the zero-order wavefunctions of $\mathbb{V}_{j+}(\chi_j)$ and $\mathbb{V}_{j-}(\chi_j)$. The Raman counterpart at 81 cm^{-1} for KH_2PO_4 at 310 K and atmospheric pressure (P_a) [27], suggests that $h\nu_{0\pm}$ is temperature and pressure independent, as well as dispersion-free. In addition, the INS spectrum reveals a doublet at $h\nu_{1+} = (24\pm2)$ meV/(192 ± 16) cm^{-1} and $h\nu_{1-} = (32\pm2)$ meV/(256 ± 16) cm^{-1} consistent with a resonance splitting $2^{-1/2}[|1_{\Uparrow j}\rangle \pm |1_{\Downarrow j}\rangle]$ and $h\nu_{1\pm} = h\nu_{1-} - h\nu_{1+} = (64\pm32)$ cm^{-1} compares favorably with $h\nu_{0\pm}$. Because this splitting should not be observed for a symmetric double-well, $h\nu_{1\pm}$ accords with a superposition of asymmetric double-wells. In addition, the mean energy of the doublet $h(\nu_{1-} + \nu_{1+})/2 = (224 \pm 32)$ cm^{-1} suggests that $h\nu_1$ is not changed through the phase transition at high pressure. The lack of pressure effects accords with the absence of causal relationship between nuclear positions, on the one hand, $h\nu_{0\pm}$ and $h\nu_1$, on the other.

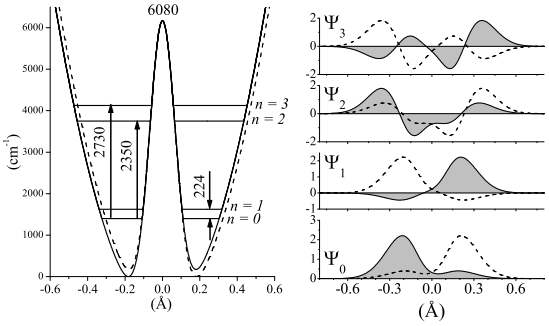

Fig. 5. Double-well operators, energy levels and eigenfunctions for the OH-stretching symmetry-species of KH_2PO_4. Solid: $\mathbb{V}_+(\chi) = 476\chi + 23484\chi^2 + 7074\exp(-106\chi^2)$. Dashed: $\mathbb{V}_-(\chi) = -476\chi + 23484\chi^2 + 7074\exp(-106\chi^2)$. $\mathbb{V}$ and χ are in cm^{-1} and Å units, respectively. The oscillator mass is 1 amu. The minima are at ±0.182 Å.

The eigenstates of interest for the ferroelectric crystal can be written as:

$$\left.\begin{aligned} |0_{\Uparrow j}\rangle &= \cos\theta^{\mathrm{H}}|\psi^{\mathrm{H}}_{\Uparrow Lj}\rangle + \sin\theta^{\mathrm{H}}|\psi^{\mathrm{H}}_{\Uparrow Rj}\rangle; \\ |1_{\Uparrow j}\rangle &= -\sin\theta^{\mathrm{H}}|\psi^{\mathrm{H}}_{\Uparrow Lj}\rangle + \cos\theta^{\mathrm{H}}|\psi^{\mathrm{H}}_{\Uparrow Rj}\rangle; \\ |0_{\Downarrow j}\rangle &= \sin\theta^{\mathrm{H}}|\psi^{\mathrm{H}}_{\Downarrow Lj}\rangle + \cos\theta^{\mathrm{H}}|\psi^{\mathrm{H}}_{\Downarrow Rj}\rangle; \\ |1_{\Downarrow j}\rangle &= -\cos\theta^{\mathrm{H}}|\psi^{\mathrm{H}}_{\Downarrow Lj}\rangle + \sin\theta^{\mathrm{H}}|\psi^{\mathrm{H}}_{\Downarrow Rj}\rangle. \end{aligned}\right\} \quad (4)$$

ψ^{H}_{Lj} and ψ^{H}_{Rj} are the eigenfunctions for polynomial expansions of the double-well around minima L_j and R_j, respectively. $\tan 2\theta^{\mathrm{H}} = \nu_{0\pm}/(\nu_1 - \nu_{0\pm})$ yields the mixing angle $\theta^{\mathrm{H}} = (15 \pm 5)^\circ$ and the delocalization degree $\sin\theta^{\mathrm{H}} = 0.26 \pm 0.08$. The same operator yields $\theta^{\mathrm{D}} \approx 2^\circ$ and $\sin\theta^{\mathrm{D}} \approx 0.03$ for an effective mass of 2 amu (Table 1). The ground state is localized to order $\sin^2\theta$ at the preferred site for parallel polarization $\langle L_{\Uparrow j}\rangle = \langle 0_{\Uparrow j}|\chi_j|0_{\Uparrow j}\rangle$. $|1_{\Uparrow j}\rangle$ at $h\nu_1$ is localized at the less favoured site for parallel polarization $\langle R_{\Uparrow j}\rangle$. $|0_{\Downarrow j}\rangle$ at V_0 and $|1_{\Downarrow j}\rangle$ at $V_0 + h\nu_1$ are localized at $\langle R_{\Downarrow j}\rangle$ and $\langle L_{\Downarrow j}\rangle$, respectively.

The ferroelectric-scheme of the four species is comprised of 32 eigenvectors and 8 distinct energy-levels (Ta-

ble 2). Only 4 eigenstates make contact with configurations in x-space. $\sum_j \mathcal{N}_0\langle 1_{\Uparrow j}|\chi_j|1_{\Uparrow j}\rangle/2 = \langle R_{\Uparrow}\rangle$ and $\sum_j \mathcal{N}_0\langle 0_{\Downarrow j}|\chi_j|0_{\Downarrow j}\rangle = \langle R_{\Downarrow}\rangle$, are in contact with R, i.e. one proton at every R_{il}. They are degenerate in energy and hence $V_0 = 4h\nu_1$. $\sum_j \mathcal{N}_0\langle 0_{\Uparrow j}|\chi_j|0_{\Uparrow j}\rangle/2 = \langle L_{\Uparrow}\rangle$ and $\sum_j \mathcal{N}_0\langle 1_{\Downarrow j}|\chi_j|1_{\Downarrow j}\rangle/2 = \langle L_{\Downarrow}\rangle$ are in contact with L, i.e. one proton at every L_{il}. The other eigenstates have no counterpart in x-space. From the contact points it follows $\sum_i |\Delta x_{i0}|^2 = \sum_j |\Delta\chi_{j0}|^2$, where the Δx_{i0}'s are distances between proton sites and the $\Delta\chi_{j0}$'s are inter-well distances. Consequently, the effective mass for every χ_j is strictly 1 amu for KH_2PO_4, or 2 amu for KD_2PO_4. This contrasts with the undetermined masses of normal coordinates in classical mechanics. This is also different in nature from circumstantial adiabatic separation of light and heavy nuclei. From Table 2 we deduce that the molar energy is $4\mathcal{N}_0h\nu_1$ for transfer-assisted flip $\langle L_{\Uparrow}\rangle \longleftrightarrow \langle R_{\Downarrow}\rangle$ or $8\mathcal{N}_0h\nu_1$ (≈ 2700 K) for adiabatic flip $\langle L_{\Uparrow}\rangle \longleftrightarrow \langle L_{\Downarrow}\rangle$.

3.2 The phase-transition temperature

If the eigenstates were pre-existing to measurements, Table 2 would not suggest any mechanism for the phase-transition, inasmuch as there is no ordering/disordering factor. From condensate viewpoint, for each χ_j of the ferroelectric $KH_{2(1-\rho)}D_{2\rho}PO_4$ quantum condensation of $(1-\rho)\mathcal{N}_0$ and $\rho\mathcal{N}_0$ phonons for protons and deuterons yields orthogonal state-vectors, say $a_{\rm H}|{\rm H}\rangle$, $a_{\rm D}|{\rm D}\rangle$, $\langle {\rm D}|{\rm H}\rangle = 0$, which can be projected onto electrically distinct vectors according to (4), say $a_{\rm H}\cos\theta^{\rm H}|{\rm H}_{\Uparrow}\rangle$ and $a_{\rm H}\sin\theta^{\rm H}|{\rm H}_{\Downarrow}\rangle$, such that $\langle {\rm H}_{\Uparrow}|{\rm H}_{\Uparrow}\rangle = \langle {\rm H}_{\Downarrow}|{\rm H}_{\Downarrow}\rangle = N\mathcal{N}_0$; $\langle {\rm H}_{\Uparrow}|{\rm H}_{\Downarrow}\rangle = 0$; $\langle {\rm H}_{\Uparrow}|\mathcal{P}|{\rm H}_{\Uparrow}\rangle = \mathbf{P}^{\rm H}_{\Uparrow}$; $\langle {\rm H}_{\Downarrow}|\mathcal{P}|{\rm H}_{\Downarrow}\rangle = \mathbf{P}^{\rm H}_{\Downarrow}$; and likewise $|{\rm D}_{\Uparrow}\rangle$ or $|{\rm D}_{\Downarrow}\rangle$ with $\theta^{\rm D} \approx 0$. Because of the continuous space-time symmetry, there is no need to distinguish fermions or bosons. The condensate vector reads:

$$|\Uparrow(\rho,P)\rangle = a_{\rm H}\left[\cos\theta^{\rm H}(\rho,P)|{\rm H}_{\Uparrow}\rangle + \sin\theta^{\rm H}(\rho,P)|{\rm H}_{\Downarrow}\rangle\right] + a_{\rm D}|{\rm D}_{\Uparrow}\rangle. \quad (5)$$

Below T_0, the eigenenergy can be partitioned as

$$E_{\Uparrow}(\rho,\mathcal{T},P) = N\mathcal{R}\mathcal{T}/2 + \Xi(\rho)P + \mathcal{E}(\rho,\mathcal{T},P\ldots). \quad (6)$$

Here $\mathcal{T} = T$, $N\mathcal{R}/2 \approx 100$ J mol^{-1} K^{-1}, $\Xi(\rho)$ is the elastic modulus and $\mathcal{E}$ accounts for further contributions, e.g. electric polarization, thermal expansion, etc, which are barely known. However, if we focus on the phase transition, the heat-capacity of KD_2PO_4 measured in the range 211−239 K is virtually a constant, viz (100±2) J mol^{-1} K^{-1}, except in the range $T_0 \pm 0.1$ K, due to latent-heat transfer [3,4]. This can be represented by a smooth function $\mathcal{E}$ that is nearly a constant between T_0-10 K and T_0+20 K and a very sharp peak at T_0 that is explained separately in Sect. 3.3. A comprehensive rationale outside this temperature-range is beyond the scope of the present work. We assume a similar behavior for KH_2PO_4.

Upon increasing $T \longrightarrow T_0$, the transition occurs when $E_{\Uparrow}$ matches an appropriate antiparallel ferroelectric level in Table 2, scaled by $\mathcal{N}_0$. We can thus distinguish two

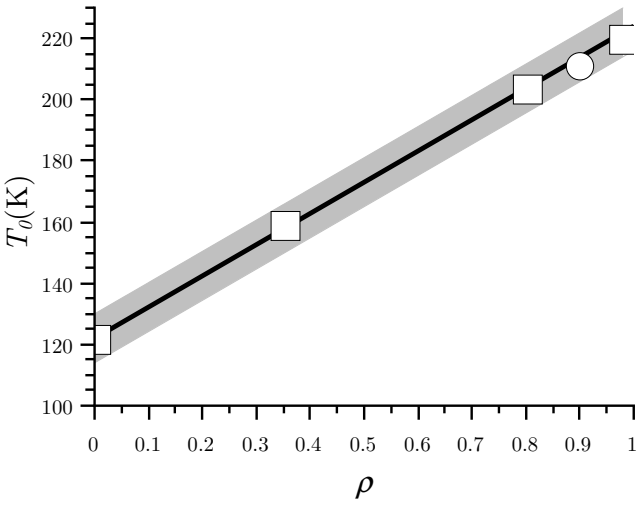

Fig. 6. Phase-transition temperatures of $KH_{2(1-\rho)}D_{2\rho}PO_4$ at atmospheric pressure. □: from [7]. ◯: from [38]. Solid: $T_0 = (122 + 102\rho)$ K. The grey zone represents statistical uncertainties for observables.

mechanisms. For KH_2PO_4 at P_a the transition to the non-polar antisymmetric superposition of electrically-distinct condensates, viz $2^{-1/2}[|{\rm H}_{\Uparrow}\rangle - |{\rm H}_{\Downarrow}\rangle]$, occurs via the antisymmetric states at $N\mathcal{R}\mathcal{T}_0/2 = 4\mathcal{N}_0h\nu_1 + 2\mathcal{N}_0h\nu_{0\pm}\sin 2\theta^{\rm H}$, where $\sin 2\theta^{\rm H}$ is the overlap for wavefunctions $\Uparrow$ and $\Downarrow$. For KD_2PO_4, the transition to a mixture of electrically-distinct condensates, say $2^{-1/2}[|{\rm D}_{\Uparrow}\rangle\langle{\rm D}_{\Uparrow}| + |{\rm D}_{\Downarrow}\rangle\langle{\rm D}_{\Downarrow}|]$, occurs at $N\mathcal{R}\mathcal{T}_0/2 = 8\mathcal{N}_0h\nu_1$. For $KH_{2(1-\rho)}D_{2\rho}PO_4$ at P_a, a linear combination of these mechanisms yields

$$N\mathcal{R}\mathcal{T}_0(\rho)/2 = 4\mathcal{N}_0h\nu_1(1+\rho) + 2(1-\rho)\mathcal{N}_0h\nu_{0\pm}\sin 2\theta^{\rm H}. \quad (7)$$

Under pressure, $E_{0_\Downarrow,0_\Downarrow,0_\Downarrow,0_\Downarrow} - E_{0_\Uparrow,0_\Uparrow,0_\Uparrow,0_\Uparrow} = 4\mathcal{N}_0h\nu_1(1+\rho) - \Xi P$, so

$$\tan 2\theta^{\rm H}(\rho,P) = \frac{(1-\rho)\nu_{0\pm}}{(1+\rho)\nu_1\left[1-\dfrac{P}{P_B(\rho)}\right] - (1-\rho)\nu_{0\pm}}. \quad (8)$$

P_B is the boundary pressure for ferroelectricity. Finally:

$$\left.\begin{array}{l} \mathcal{T}_0(\rho,P) = \\ \dfrac{2\mathcal{N}_0}{N\mathcal{R}}[\Delta E(\rho,P) + 2(1-\rho)h\nu_{0\pm}\sin 2\theta^{\rm H}]; \\ \Delta E(\rho,P) = 4h\nu_1\left\{(1+\rho)\left[1-\dfrac{P}{P_B(\rho)}\right]\right. \\ \left. - 2(1-\rho)[\sin^2\theta^{\rm H}(\rho,P) - \sin^2\theta^{\rm H}(\rho,0)]\right\}; \\ P_B(\rho) = \\ \dfrac{\mathcal{N}_0}{\Xi(\rho)}[(1+\rho)4h\nu_1 + 2(1-\rho)h\nu_{0\pm}]. \end{array}\right\} \quad (9)$$

This deterministic law accounts for classical measurements at the macroscopic level, to within experimental precision. It depends on two microscopic observables ($h\nu_{0\pm}$,

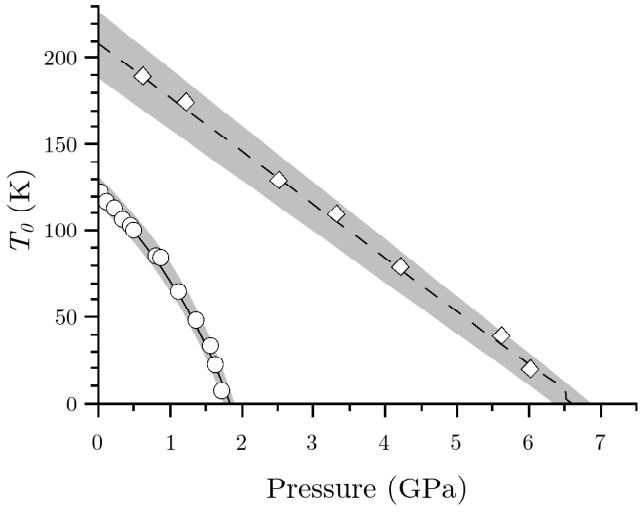

Fig. 7. Pressure effects on the phase-transition temperature of $KH_{2(1-\rho)}D_{2\rho}PO_4$. ∘: measurements for $\rho = 0$ digitized from [6]. ⋄: measurements for $\rho = 0.8$ digitized from [10]. Solid: calculated according to (9) with $P_B(0) = (3.5 \pm 0.2)$ GPa. Dashed: (9) with $P_B(0.86) = (6.8 \pm 0.2)$ GPa. The grey zones represent statistical uncertainties for observables.

$h\nu_1$) and two macroscopic parameters (ρ, P_B). $\Xi(\rho)$ is nearly ρ-independent and there is no evidence of any significant change of $\mathcal{E}$ across the transition, whatever ρ and P. The linear isotope effect (fig. 6) mirrors the superposition of isotopically-distinct condensates. The nonlinear pressure effect for KH_2PO_4 (fig. 7) witnesses superposition of electrically-distinct condensates for protons. (A similar nonlinear effect has been reported for $NH_4H_2PO_4$ [6].) The quasi-linear pressure effect for $\rho = 0.8$ accords with $\theta^{\mathrm{D}} \approx 0$. It transpires that $h\nu_1$ is independent of ρ and P. The lack of pressure effect confirms that $h\nu_1$ and $\mathcal{T}_0$ do not depend on nuclear positions (geometric effect). The lack of mass effect is at variance with Table 1. This suggests that a causal relationship between the electric field and the potential operators keeps $h\nu_1$ at a constant value, via changes of the magnitude of the asymmetry parameter and of the inter-well distance upon deuteration. At the same time, mass effects on $h\nu_2$ or $h\nu_3$ suggest that the quadratic term and the Gaussian barrier are not significantly changed.

3.3 The phase-transition mechanism and the latent heat

The phase-transition of KH_2PO_4 at P_a can be represented by the isothermal variation of the mixing angle φ ($\theta^{\mathrm{H}} \leq \varphi \leq \pi/4$) for Bloch-states $\Uparrow$ and $\Downarrow$. Heat transfer to the ferroelectric-phase can be sketched out as:

$$\left.\begin{array}{ll}
& \cos\theta^{\mathrm{H}}|\mathrm{H}_{\Uparrow}\rangle + \sin\theta^{\mathrm{H}}|\mathrm{H}_{\Uparrow}\rangle \\
& (+N\mathcal{R}\mathcal{T}_0/2 + \Delta H_l^{\mathrm{H}}) \\
\longrightarrow & \dfrac{\mathcal{N}_0^2}{4}\bigotimes_j[\cos\theta^{\mathrm{H}}|\psi^{\mathrm{H}}_{\Uparrow Lj}\rangle + \sin\theta^{\mathrm{H}}|\psi^{\mathrm{H}}_{\Uparrow Rj}\rangle \\
& -(\cos\theta^{\mathrm{H}}|\psi^{\mathrm{H}}_{\Downarrow Rj}\rangle + \sin\theta^{\mathrm{H}}|\psi^{\mathrm{H}}_{\Downarrow Lj}\rangle)] \\
& (+N\mathcal{R}\mathcal{T}_0/2 + \Delta H_l^{\mathrm{H}}) \qquad \mathbb{II} \\
\longrightarrow & \dfrac{\mathcal{N}_0^2}{4}\bigotimes_j\{a_0[\cos\varphi_0|\psi^{\mathrm{H}}_{\Uparrow Lj}\rangle + \sin\varphi_0|\psi^{\mathrm{H}}_{\Uparrow Rj}\rangle \\
& -(\cos\varphi_0|\psi^{\mathrm{H}}_{\Downarrow Rj}\rangle + \sin\varphi_0|\psi^{\mathrm{H}}_{\Downarrow Lj}\rangle)] \\
& +a_1[-\sin\varphi_0|\psi^{\mathrm{H}}_{\Uparrow Lj}\rangle + \cos\varphi_0|\psi^{\mathrm{H}}_{\Uparrow Rj}\rangle \\
& -(\sin\varphi_0|\psi^{\mathrm{H}}_{\Downarrow Rj}\rangle - \cos\varphi_0|\psi^{\mathrm{H}}_{\Downarrow Lj}\rangle)]\} \\
& (+\Delta H_l^{\mathrm{H}}) \qquad \mathbb{III} \\
\longrightarrow & \dfrac{1}{\sqrt{2}}[|\Uparrow(0,P)\rangle - |\Downarrow(0,P)\rangle] \qquad \mathbb{IIII}
\end{array}\right\} \quad (10)$$

Step $\mathbb{I}$: iso-energy breakdown of the time-translation symmetry via resonance. Step $\mathbb{III}$: internal conversion of the kinetic energy, ie $Nk\mathcal{T}_0/8$ per χ_j, into potential energy yields a superposition at $\mathcal{T}_0$ with $|a_0|^2 = (1+a)^{-1}$; $|a_1|^2 = |a_0|^2 a$; $a = \exp -h\nu_1/k\mathcal{T}_0$. From the greater energy cost for antisymmetrization, ie $\mathcal{N}_0 h\nu_1$ (symmetrization) $+\mathcal{N}_0 h\nu_{0\pm}$ (antisymmetrization), than that of the phase-transition, $\mathcal{N}_0(h\nu_1 + \frac{1}{2}h\nu_{0\pm}\sin 2\theta^{\mathrm{H}})$, we deduce φ_0, as well as the occupancy ratio, $R_0^{\mathrm{H}} = R_{\Uparrow j}/L_{\Uparrow j} = R_{\Downarrow j}/L_{\Downarrow j}$, and the entropy $\mathcal{S}(R_0^{\mathrm{H}})$ at $\mathcal{T}_0$:

$$\left.\begin{array}{rl}
\tan 2\varphi_0 = & \dfrac{\nu_{0\pm}}{(\nu_1 - \nu_{0\pm})\left[1 - \dfrac{\mathcal{T}_0}{\mathcal{T}_{0-}}\right]}; \\
R_0^{\mathrm{H}} = & \dfrac{\sin^2\varphi_0 + \cos^2\varphi_0 \exp -\dfrac{h\nu_1}{k\mathcal{T}_0}}{\cos^2\varphi_0 + \sin^2\varphi_0 \exp -\dfrac{h\nu_1}{k\mathcal{T}_0}}; \\
\mathcal{S}(R_0^{\mathrm{H}}) = & \dfrac{\ln(1+R_0^{\mathrm{H}})}{(1+R_0^{\mathrm{H}})} + \dfrac{R_0^{\mathrm{H}}}{(1+R_0^{\mathrm{H}})}\ln\dfrac{(1+R_0^{\mathrm{H}})}{R_0^{\mathrm{H}}};
\end{array}\right\} \quad (11)$$

where $\mathcal{T}_{0-} = 8(h\nu_1 + h\nu_{0\pm})/k$. Step $\mathbb{IIII}$: latent-heat transfer $\Delta H_l^{\mathrm{H}} = 2\mathcal{R}\mathcal{T}_0[\ln 2 - \mathcal{S}(R_0^{\mathrm{H}})]$ yields a dielectric condensate at $\mathcal{T} = 0$ K.

On the other hand, the nonresonant mechanism for KD_2PO_4 reads

$$\left.\begin{array}{ll}
& |\mathrm{D}_{\Uparrow}\rangle \ (+NRT_0/2 + \Delta H_l^{\mathrm{D}}) \\
\longrightarrow & \dfrac{\mathcal{N}_0^2}{4}\bigotimes_j\left[a_0|\psi^{\mathrm{D}}_{\Uparrow Lj}\rangle + a_1|\psi^{\mathrm{D}}_{\Uparrow Rj}\rangle\right] \\
& (+\Delta H_l^{\mathrm{D}}) \qquad \mathbb{I} \\
\longrightarrow & \dfrac{1}{\sqrt{2}}[|\mathrm{D}_{\Uparrow}\rangle\langle\mathrm{D}_{\Uparrow}| + |\mathrm{D}_{\Downarrow}\rangle\langle\mathrm{D}_{\Downarrow}|] \qquad \mathbb{III}.
\end{array}\right\} \quad (12)$$

Step $\mathbb{I}$: interconversion yields $R_0^{\mathrm{D}} = \exp -h\nu_1/k\mathcal{T}_0 = e^{-3/2}$. Step $\mathbb{III}$: latent-heat transfer $\Delta H_l^{\mathrm{D}} = \mathcal{R}\mathcal{T}_0[\ln 2 - \mathcal{S}(R_0^{\mathrm{D}})]$ yields a mixed condensate at $\mathcal{T} = 0$ K.

Calorimetric measurements accord with the proposed mechanisms, as well as with the assignment of $h\nu_{0\pm}$ and

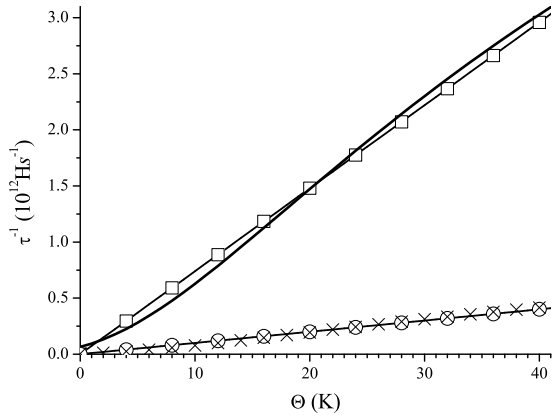

Fig. 8. Comparison of observed and calculated relaxation rate τ^{-1} in proton per second units (Hs^{-1}) for $KH_{2(1-\rho)}D_{2\rho}PO_4$ at $\Theta = T - T_0$. Solid with □: $\tau^{-1} = 9.1 \times 10^{12}(T/T_0 - 1)$ Hs^{-1} for KH_2PO_4, from [38]. Solid: $\tau^{-1} = 9.6 \times 10^{12} \exp[-60/(\Theta + \Theta_{0\pm})]$ Hs^{-1} (14). $T_0 = 122$ K. $\Theta_{0\pm} = (12 \pm 4)$ K. Solid with ◯: $\tau^{-1} = 1.22 \times 10^{12}(T/T_0 - 1)$ Hs^{-1} for $\rho \approx 0.9$ from [38]. Solid with X: $\tau_{H1}^{-1} = 1.35 \times 10^{12} \exp[-60/(\Theta + \Theta_{0\pm})]$ Hs^{-1} (14). $T_0 = 211$ K. $\Theta_{0\pm} = (11 \pm 4)$ K.

$h\nu_1$. For KH_2PO_4 at P_a, $\mathcal{T}_{0-} = (152 \pm 16)$ K, $\mathcal{T}_0/\mathcal{T}_{0-} = 0.80 \pm 0.05$, $\varphi_0^{\rm H} = (35 \pm 4)°$, $R_0^{\rm H} = 0.63 \pm 0.08$ and $|\Delta H_l^{\rm H}| = 43_{-13}^{+40}$ $\mathrm{J\,mol^{-1}}$ accords with $46.2_{-6.0}^{+4.5}$ $\mathrm{J\,mol^{-1}}$ measured [4]. In the case of KD_2PO_4, $|\Delta H_l^{\rm D}| = (406 \pm 40)$ $\mathrm{J\,mol^{-1}}$ compares favorably with (440.3 ± 2.8) $\mathrm{J\,mol^{-1}}$ measured for $\rho = 0.97$ [3]. The latent-heats effectively measured accord with a first-order quantum transition between a ferroelectric condensate at $\mathcal{T}_0$ and either a superposition (KH_2PO_4) or a mixture (KD_2PO_4) of condensates at 0 K. Above T_0 the crystal is in contact with a thermal bath at T, while the eigentemperature of the condensate is $\Theta = T - T_0$. The condensate is stabilized. There is no significant entropy jump for heavy nuclei which can be regarded as a mere energy-reservoir switching on/off the polarization.

As a sequel of this discussion, the spontaneous polarization of the ferroelectric condensate measured under static conditions should be temperature independent: $|\mathbf{P}_{dc}| = (1-\rho)|\mathbf{P}^{\rm H}|\cos 2\theta^{\rm H} + \rho|\mathbf{P}^{\rm D}|$. At T_0 we anticipate a discontinuous jump to $|\mathbf{P}_{dc}| = [(1-\rho)|\mathbf{P}^{\rm H}|\cos 2\varphi_0 + \rho|\mathbf{P}^{\rm D}|][1 - \exp -(h\nu_1/k\mathcal{T}_0)]$ and then a continuous decrease to zero during latent-heat transfer. Alternatively, the saturation polarization measured with an ac-field, ie $|\mathbf{P}_{ac}| = [(1-\rho)|\mathbf{P}^{\rm H}|\cos 2\varphi + \rho|\mathbf{P}^{\rm D}|][1 - \exp -(h\nu_1/k\mathcal{T})]$, should vary continuously with $\mathcal{T}$. This is in qualitative agreement with reported measurements [7].

3.4 Relaxometry

For a nonpolar condensate at $\Theta \ll h\nu_1/k$, off-resonance energy-transfer realizes at the time $t = 0$ of the event a transitory superposition of proton and deuteron eigenstates:

$$a_{\rm H}[\alpha_{0+}|0_+\rangle_{\rm H} + \alpha_{0-}|0_-\rangle_{\rm H}] + a_{\rm D}[|0_\Uparrow\rangle_{\rm D} + |0_\Downarrow\rangle_{\rm D}]. \quad (13)$$

The eigentemperature is $\Theta + \Theta_{0\pm}$, where $(1-\rho)Nk\Theta_{0\pm}$ is the energy temporarily borrowed from the condensate in order to realize the splitting $2(1-\rho)h\nu_{0\pm}$. Hence: $|\alpha_{0+}|^2 = (1+\alpha)^{-1}$; $|\alpha_{0-}|^2 = \alpha|\alpha_{0+}|^2$; $\alpha = \exp[-h\nu_{0\pm}/k(\Theta+\Theta_{0\pm})]$; $\Theta_{0\pm} = 2h\nu_{0\pm}/Nk = (10 \pm 2)$ K. The critical relaxation rate is then

$$\left.\begin{aligned} \tau_{\rm H1}^{-1}(\rho) &= 4(1-\rho)\nu_{0\pm}\alpha^{1/2} \\ &= 4(1-\rho)\nu_{0\pm}\exp\frac{-h\nu_{0\pm}}{2k(\Theta+\Theta_{0\pm})} \end{aligned}\right\} \quad (14)$$

and $4\nu_{0\pm} = (9.6 \pm 2.0)10^{12}s^{-1}$. In contrast with the statistical viewpoint [93], the deterministic relaxation-rate follows from quantum interferences.

The Curie-Weiss law reported for KH_2PO_4 can be regarded as a linear approximation of (14) (fig. 8). Best fit exercises yield $\Theta_{0\pm} = (12 \pm 4)$ K, in reasonable agreement with the expected value, and there is no evidence of overdamping due to decoherence. The relaxation rate highlights the decoupling of the eigentemperature of the condensate from the temperature of the environment. In fact, we can distinguish three temperatures: T for the surroundings, Θ for the condensate and $\Theta + \Theta_{0\pm}$ for the induced state.

The Curie-Weiss law reported for $\rho \approx 0.9$ is also in accordance with (14) (fig. 8). From the measured slope, ie $(1.35 \pm 0.3)10^{12}s^{-1}$, we estimate $\rho = 0.86 \pm 0.09$ and $\Theta_{0\pm} = (11 \pm 4)$ K. This isotope effect is distinctive of nonseparable proton-deuteron states.

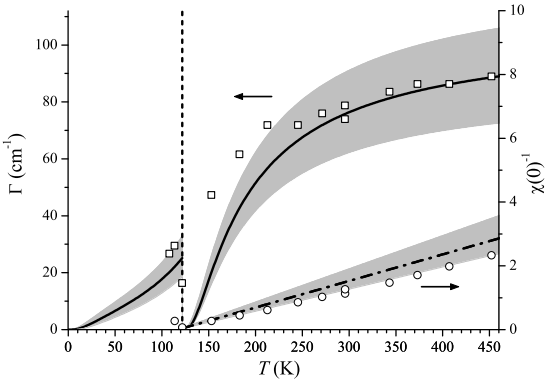

Fig. 9. Comparison of observed and calculated half-width at half-height of the central peak (Γ left-hand-side axis) and of the observed and calculated reciprocal zero-frequency susceptibility ($\chi(0)^{-1}$ right-hand-side axis). □ and ◯: digitized from [32]. Dashed: $T_0 = 122$ K. Solid: Γ calculated according to (15) for $T \geq T_0$ or (16) for $T \leq T_0$. Dot dashed: $\chi(0)^{-1} = 2k(\Theta + \Theta_{0\pm}/2)/h\nu_{0\pm}$. The grey zones represent statistical uncertainties for observables.

We deduce from (14) the Lorentzian-profile measured for B_2-species via polarized Raman:

$$\left.\begin{aligned} L(\omega) &= \frac{1}{\pi}\frac{\tau_{\rm H2}}{1+\omega^2\tau_{\rm H2}^2}; \\ \tau_{\rm H2}^{-1}(\rho) &= 2(1-\rho)\nu_{0\pm}\exp\frac{-h\nu_{0\pm}}{2k(\Theta+\Theta_{0\pm}/2)}. \end{aligned}\right\} \quad (15)$$

The half-width at half-height, $\Gamma = (\pi\tau_{H2})^{-1}$, decreases with Θ and the intensity at the maximum diverges. For $\rho = 0$, the reciprocal zero-frequency susceptibility obeys a Curie-Weiss law: $\chi^{-1} = 1/\ln(\tau_{H2}/\tau_{0\pm}) = 2k(\Theta+\Theta_{0\pm}/2)/h\nu_{0\pm}$. This is in qualitative agreement with observations (fig. 9) and the "clamped Curie-temperature" of 117 K reported by several authors [32,34,35] accords with $\Theta_{0\pm}/2 = 5$ K. In addition, the relaxation rate anticipated below T_0,

$$\tau_{H3}^{-1}(\rho) = 2(1-\rho)\nu_{0\pm}\tan\varphi(\mathcal{T})\exp\frac{-h\nu_{0\pm}}{2k(\mathcal{T}+\Theta_{0\pm}/2)}, \quad (16)$$

accounts for resurgence of the central peak (fig. 9). The discontinuity at T_0 is primarily due to the eigentemperature jump, while the φ-jump is of marginal consequence. Raman data suggest with substantial uncertainties that the central peak could be the counterpart of measurement-induced instabilities revealed with a much better precision by time-resolved stimulated Raman.

3.5 Neutron Compton scattering

A NCS event breaks space-time-translation symmetry via off-resonance energy-transfer on the eV-scale and momentum transfer in the range $30-100$ Å^{-1}. A Compton profile mirrors a snapshot on the $\sim 10^{-15}s$ timescale of the probability density $n(p)$ along $\mathbf{Q}$. For KH_2PO_4 and $\mathbf{Q}$ parallel to O$\cdots$O, Reiter et al. [41] have reported a decrease above T_0 of the variance $\sigma_\parallel$ of $n(p_\parallel)$, that is not observed for the deuterium enriched crystal [42].

In statistical physics, $n(p)$ is the Fourier-transform of spontaneous fluctuations, on the assumption that neutron scattering is a very weak process measuring the properties of the unperturbed system. Within the condensate framework, pre-existing fluctuations in direct space are ruled out. For KH_2PO_4 at $\mathcal{T} \ll h\nu_1/k$ (below T_0), or at $\Theta \ll h\nu_{0\pm}$ (above T_0), the measurement-induced density is $n_0(p_\parallel) = \sum_j |a_j\varphi_0(p_j)|^2$, where $\sum_j |a_j|^2 = 1$ and $\varphi_0(p_j)$ is the Fourier-transform of the ground-state wavefunction $\psi_0(\chi_j)$. Hence $n_0(p_\parallel) = |\varphi_0(p)|^2$ and $\sigma_\parallel$ can be confronted with $\langle p^2\rangle^{1/2} = \langle\varphi_0|p^2|\varphi_0\rangle^{1/2}$.

For KH_2PO_4 at $T_0 - 30$ K, $\sigma_{H||} = 5.69$ Å^{-1} accords with $\langle p_H^2\rangle^{1/2} = (5.7 \pm 0.3)$ Å^{-1} computed for $|0_{\Uparrow j}\rangle$ with a basis-set of 40 harmonic eigenfunctions. At $T_0 + 10$ K, $\sigma_{H||} = 5.51$ Å^{-1} is also in accordance with $\langle p_H^2\rangle^{1/2} = (5.4 \pm 0.3)$ Å^{-1} computed for $2^{-1/2}[|0_{\Uparrow j}\rangle + |0_{\Downarrow j}\rangle]$. This reasonably good agreement confirms both the assignment scheme (Table 1) and the superposition of asymmetric double-wells above T_0. If the potential operator were single-well below T_0, then $\langle p_H^2\rangle^{1/2}$ would be ≈ 6.2 Å^{-1}. The rather modest delocalization degree below T_0 decreases the variance by ≈ 0.5 Å^{-1}, while full delocalization above T_0 yields a further decrease by only ≈ 0.3 Å^{-1}.

The symmetric double-well potential above T_0 posited by Reiter et al. [41] (Table 3) is forbidden by space-group symmetry. In addition, even if we envisage a transitory measurement-induced violation of the symmetry, instead of a pre-existing Born-Oppenheimer potential, the reported tunnel splitting $h\nu_t \approx 94$ meV (≈ 750 cm^{-1}) is definitively not observed through INS [40] and yields $\langle p_H^2\rangle^{1/2} = 4.48$ Å^{-1}, that is substantially different from 5.51 Å^{-1} measured. The authors argued that $h\nu_t \approx 10 \times kT_0 \approx 800$ cm^{-1} is a necessary condition to account for interferences in the tail of the distribution, which are visible only if the population of the upper tunneling state is negligible. Our counter argument consistent with symmetry, INS and NCS is that such a huge splitting is not necessary for a condensate at $\Theta \approx 10$ K ($h\nu_{0\pm}/k\Theta \approx 12$).

For the deuterium enriched crystal, Reiter et al. [42] have omitted some crucial informations necessary for a fair assessment of their data. They do not mention any measurement (eg diffraction) proving that the crystal was properly oriented and had effectively transited at the claimed $T_0 = 229$ K, that is greater than the upper bound in fig. 6. The size of the crystal and the isotope composition are omitted. More important, while Compton profiles at $m = 1$ amu and 2 amu were automatically measured for every single run of the time-of-flight technique, the profile at 1 amu is ignored. The reported $\sigma_{D\parallel}(\rho) = 5.58$ Å^{-1} at $T_0 - 40$ K or 5.47 Å^{-1} at $T_0 + 10$ K are quite different from $\langle p_D^2\rangle^{1/2} = (7.4 \pm 0.3)$ Å^{-1} computed for an effective mass of 2 amu (Table 1), irrespective of the phase transition. In addition, $\sigma_{D\parallel}(\rho) < \sigma_{H\parallel}$ (see Table 1 in [42]) is at variance with the harmonic model, viz $\sigma_{D\parallel} = (m_D/m_H)^{1/4}\sigma_{H\parallel}$. Reiter et al. suggest that the mass effect could be counterbalanced by markedly different potentials and propose a decidedly new assignment scheme for Raman. However, the scheme proposed by Tominaga et al. [30] is straightforward and excludes a dramatic change of the potential operator upon deuteration. In addition, there is no obvious reason to justify that the mass effect could be so precisely compensated and a fortuitous coincidence is exceedingly improbable.

From condensate viewpoint, supposing $\rho < 0.98$, neutrons scattered by entangled proton-deuteron scatterers yield identical profiles scaled by cross-sections at 1 amu or 2 amu and hence $\sigma_1(\rho) = \sigma_2(\rho)$. Pursuing the reasoning presented in Sect. 3.4, the resonance splitting above T_0 is $(1-\rho)h\nu_{0\pm}$. The deuteration effect is of marginal consequences to the variance, so $\sigma_{1\parallel}(0) - \sigma_{2\parallel}(\rho) = 0.04$ Å^{-1} is tiny. Nevertheless, interferences reported for KH_2PO_4 are hidden by the greater temperature factor $\exp[-(1-\rho)h\nu_{0\pm}/k\Theta]$. Below T_0 the delocalization degree is $(1-\rho)\sin\theta^H$. At a given temperature, deuteration should increase the variance, ie $\sigma_\parallel(\rho) > \sigma_\parallel(0)$. Yet $\sigma_{1\parallel}(0) - \sigma_{2\parallel}(\rho) = 0.11$ Å^{-1} suggests that this effect is overridden by the greater temperature factor $\exp(-h\nu_1/kT)$ of the less favored state localized in the opposite well, that is ≈ 0.03 at 100 K or ≈ 0.19 at 200 K. Consequently, $\sigma_{2\parallel}(\rho) < \sigma_{1\parallel}(0)$ and the narrowing of $\sigma_{1\parallel}(0)$ across the transition at ≈ 122 K is diminished for $\sigma_{2\parallel}(\rho)$ at ≈ 220 K.

Variances measured for single-wells perpendicular to O$\cdots$O can be associated with frequencies in the harmonic approximation: $\sigma_{1\perp}(0) = 4.14$ Å^{-1} (1115 cm^{-1}), $\sigma_{2\perp}(\rho) = 4.32$ Å^{-1} (858 cm^{-1}) at $T < T_0$, or $\sigma_{1\perp}(0) = 4.24$ Å^{-1} (1170 cm^{-1}), $\sigma_{2\perp}(\rho) = 4.33$ Å^{-1} (863 cm^{-1}) at $T > T_0$. The Raman counterparts at $T < T_0$ are 1012 cm^{-1} and

725 cm^{-1}, respectively [30]. The $\approx$ 10% difference for KH_2PO_4 is likely due to anharmonicity. The $\approx$ 17% difference for $KH_{2(1-\rho)}D_{2\rho}PO_4$ suggests a further mass effect following from entangled scatterers. If there is no unforeseen additional effect, this would be consistent with $\rho \approx 0.95$ and $T_0 \approx 219$ K. The momentum density of disentangled deuterons cannot be measured even for a high ρ-value. This drawback is seriously misleading if it is ignored.

Within the condensate framework, NCS accords with the spectroscopy-based double-well operator for KH_2PO_4. NCS and relaxometry accord with the extraordinary low temperature of the unpolarized condensate. NCS, diffraction and relaxometry accord with entangled scatterers for $KH_{2(1-\rho)}D_{2\rho}PO_4$. Any representation based on a statistical ensemble of nuclear oscillators is inappropriate.

4 Perspective

Some of the best-documented hydrogen-bonded crystals suggest that the condensates framework could be of general significance.

4.1 Potassium hydrogen carbonate

Nonferroic $KH_{(1-\rho)}D_\rho CO_3$'s demonstrate quantum correlations consistent with the notion of condensate. They undergo a reversible phase-transition ($P2_1/a \longleftrightarrow C2/m$) at temperatures ranging from $T_c \approx 318$ K for $KHCO_3$ to $T_c \approx 353$ K for $KDCO_3$ [94]. Both phases are comprised of centrosymmetric cyclic-dimers $(H_{(1-\rho)}D_\rho CO_3)_2$ parallel to (103) planes and well separate by the stacking of K-nuclei. Positional parameters and vibrational spectra are practically unchanged across the transition and disorder is excluded [79]. We are not aware of any theoretical model ever reported for the phase transition.

By analogy with $KH_{2(1-\rho)}D_{2\rho}PO_4$, let x_1 and x_2 be positional parameters for particle-like protons or deuterons along O$\cdots$O bonds of dimers and let χ_u (antisymmetric) and χ_g (symmetric) be the symmetry species. Asymmetric double-wells in χ-space account for coexistence of dimer configurations in x-space, say L_1L_2 (preferred) and R_1R_2 (less favored). The inter-site separation $r_H \approx r_D \approx 0.6$ Å and the double-well asymmetry $h\nu_1 = (216 \pm 8)$ cm^{-1} yield $h\nu_{0\pm} = (17 \pm 5)$ cm^{-1} and $\theta^H \approx 2^\circ$ [95,96].

Below T_c the long dimer-axes are alternately tilted by $\phi \approx \pm 3^\circ$ with respect to (a, c) glide-planes and the occupancy ratio is $R_1R_2 : L_1L_2 < 1$. The translation operator $(\boldsymbol{a}/2; \boldsymbol{b}/2; 0)$ transforming configurations $(L_{1+}L_{2+}, R_{1+}R_{2+}, \phi)$ into $(L_{1-}L_{2-}, R_{1-}R_{2-}, -\phi)$ is equivalent to flipping both the b-axis orientation and the asymmetry-parameter of the double-wells. Apart from electric polarization, b plays the same role as the c axis of KDP. Above T_c, glide-planes turn into mirror-planes and $R_1R_2 : L_1L_2 = 1$.

The phase-transition can be rationalized with the energy-level scheme presented in Table 4. Because there is no electric polarization, $|n_{u+}, n_{g+}\rangle$ and $|n_{u-}, n_{g-}\rangle$ for opposite orientations of b are degenerate. $|0_{u+}, 0_{g+}\rangle$ and $|1_{u+}, 1_{g+}\rangle$ are localized around $\langle L_{u+}\rangle\langle L_{g+}\rangle$ and $\langle R_{u+}\rangle\langle R_{g+}\rangle$ corresponding to $L_{1+}L_{2+}$ and $R_{1+}R_{2+}$, respectively, while $|0_{u-}, 0_{g-}\rangle$ and $|1_{u-}, 1_{g-}\rangle$ localized around $\langle R_{u-}\rangle\langle R_{g-}\rangle$ and $\langle L_{u-}\rangle\langle L_{g-}\rangle$ correspond to $R_{1-}R_{2-}$ and $L_{1-}L_{2-}$, respectively. $|1_{u+}, 0_{g+}\rangle$ and $|0_{u+}, 1_{g+}\rangle$, on the one hand, $|1_{u-}, 0_{g-}\rangle$ and $|0_{u-}, 1_{g-}\rangle$, on the other, have no counterpart in x-space. Below T_c, spontaneous symmetry-breakdown follows from quantum condensation. For $KHCO_3$, the transition occurs via tunneling at $T_c = \mathcal{N}_0 h(\nu_1 - \nu_{0\pm}/4)/\mathcal{R} = (318 \pm 12)$ K, when the kinetic energy of χ_u and χ_g matches the intermediate levels. From the jump of the ratio $R_1R_2 : L_1L_2$ at T_c, ie $\approx e^{-1} \longleftrightarrow 1$, we calculate $|\Delta H_l| \approx 280$ J mol^{-1} in reasonable agreement with ≈ 300 J mol^{-1} reported [94]. The calculated relaxation rate per proton [97] accords with measurements [98] and, because there is no interconversion of energy, there is no discontinuity at T_c. For $KDCO_3$, we deduce $h\nu_1 \approx 235$ cm^{-1} from T_c.

The condensate framework reveals significant differences. For KH_2PO_4, interconversion at T_0 of the total kinetic energy into potential energy switches on/off the electric polarization via separation/superposition of polar condensates. $h\nu_1$ is ρ-independent. For the nonferroic $KHCO_3$, only χ_u and χ_g are involved, there is no interconversion and the isotope effect on $h\nu_1$ accord with a phase transition distinctive of the hydrogen/deuterium bonds.

4.2 Tris potassium hydrogen disulfate

Crystals $K_3H_{1-\rho}D_\rho(SO_4)_2$ undergo an isostructural ferroelectric $\longleftrightarrow$ dielectric transitions at $T_0(\rho)$ ranging from 0 for $\rho <\approx 0.2$ to ≈ 85.5 K for $\rho \approx 1$. The phase transition is quantum in nature but the mechanism is markedly different from that of KDP [80]. These crystals are comprised of linear centrosymmetric-dimers, $SO_4\cdots H_{1-\rho}D_\rho\cdots SO_4$, well separate by the staking of K-nuclei. The probability density for $H_{(1-\rho)}D_\rho$ is a maximum at the bond center. $R_{OO} \approx 2.50$ Å compares with KDP but the potential operator for H-stretching is single-well. Here, the crux of the matter is that the Gaussian-like wavefunction of the ground-state for any single-well is incompatible with the crystallographic center of symmetry. Clearly, quantum condensation avoids this conflict. The same line of reasoning holds for the Rb analogue, as well as for linear centrosymmetric-dimers $H(CF_3COO)_2$ in nonferroic crystals of K or Cs hydrogen bistrifluoroacetate [99].

5 Conclusion

A crystal $KH_{2(1-\rho)}D_{2\rho}PO_4$ at thermal equilibrium is a macroscopically-quantum system in a pure state that can be projected onto a basis of four state-vectors representing electrically- and isotopically-distinct condensates with space-time-translation symmetry and zero-entropy. Nuclear positions and vibrational states are indefinite and new properties emerge. The eigentemperature $\mathcal{T}$ following

from the single-valued eigenenergy is different in nature from the thermodynamic temperature of the environment T. The phase-transition temperature highlights isotope and pressure effects on the crystal state. The latent-heat is consistent with a first-order quantum transition between a ferroelectric condensate at $\mathcal{T}_0$ and either a superposition (KH_2PO_4) or a mixture (KD_2PO_4) of condensates at $\mathcal{T} = 0$ K, via interconversioin of the eigenenergy into potential energy. There is no causal relationship between nuclear positions and either $\mathcal{T}_0$ or the latent heat.

At the microscopic level, a measurement realizes a transitory state either in the space of static positional observables or in that of the symmetry species for vibrational states. These mutually-exclusive representations rule out conflicts of interpretation arising when the outcome of a quantum measurement is regarded as a pre-existing reality, irrespective of the measuring apparatus. They account for phenomena outside the bounds of statistical physics: (i) entangled proton-deuteron scatterers are realized via diffraction, relaxometry and neutron Compton scattering; (ii) distinct proton or deuteron eigenstates are realized via spectrometry; (iii) there is no causal relationship between vibrational states and nuclear positions; (iv) the decoupling of the eigentemperature of the condensate from the temperature of the environment is attested by the extraordinary low eigentemperature of the unpolarized condensate revealed by relaxometry and NCS.

Both authors contributed equally to this paper.

Appendix A: The assignment scheme

The $\mathbb{V}_j(\chi_j)$'s are modelled for every χ_j with identical asymmetric double-wells comprised of a quadratic function, a Gaussian barrier and a linear asymmetry (fig. 5 and Table 1). They follow from the assignment-scheme of the vibrational spectra of KH_2PO_4 and $KH_{2(1-\rho)}D_{2\rho}PO_4$, inspired by those previously reported for $KHCO_3$ [95,100] or benzoic acid (C_6H_5COOH) [77,78]. The chosen analytical function and the proposed assignment-scheme are consistent with measurements examined in Secs 3.2 to 3.5.

(I) We tentatively assign the broad Raman band reported by Tominaga et al. [30] in the $2300 - 2400$ cm^{-1} range to $h\nu_2$ $(0 \longrightarrow 2)$ and that in the $2680 - 2780$ cm^{-1} range to $h\nu_3$ $(0 \longrightarrow 3)$ [101]. The precision is severely limited by bandwidths exceeding 500 cm^{-1}. Consequently, unresolved transitions for different χ_j's are supposed to be degenerate. As expected, $h\nu_2$ and $h\nu_3$ are at lower energies than those reported for longer O···O bonds in $KHCO_3$ (2475, 2820 cm^{-1}, $R_{OO} = 2.58 - 2.60$ Å) or benzoic acid (2570, 2840 cm^{-1}, $R_{OO} = 2.61 - 2.65$ Å).

(II) We seek after $h\nu_1$ $(0 \longrightarrow 1)$ in the INS spectrum of ferroelectric KH_2PO_4 [40], knowing that the total nuclear cross-section for protons, $2\sigma_H \approx 164$ bn, is much greater than that for other nuclei, $\sigma_{KPO_4} \approx 20$ bn. By analogy with $h\nu_1 = (216 \pm 5)$ cm^{-1} for $KHCO_3$, or (172 ± 4) cm^{-1} for BA, we tentatively assign to $h\nu_1$ the INS band of KH_2PO_4 reported at (28 ± 2) meV, ie (224 ± 16) cm^{-1}. This band was attributed to PO_4-librations by Belushkin and Adams [40], but our counterargument is that there is no visible counterpart in Raman [28,29]. Transitions for different χ_j's are degenerate.

(III) Finally, setting the effective mass to 1 amu, one and the same double-well operator is fully determined for every χ_j, yet with substantial uncertainty. The parameters were adjusted in order to minimize the mean-square difference between observations and energy levels computed with a basis-set of 40 harmonic wavefunctions [99].

The Raman spectra of $KH_{2(1-\rho)}D_{2\rho}PO_4$ reveal separate H and D states for $n = 2, 3$, and frequency shifts suggest a prominent mass-effect [30]. There is no evidence to suggest any significant change of the potential function. On the other hand, $h\nu_1$ is not visible for deuterons. The expected frequency shift is rather modest (Table 1) and it will transpire in Sect. 3.2 that $h\nu_1$ is unaffected by deuteration.

References

1. G. Busch and P. Scherrer. Eine neue seignette-electrische substanz. *Naturwiss.*, 23:735, 1935.
2. Kaminow I P. Microwave dielectric properties of $NH_4H_2P0_4$, KH_2As0_4, and partially deuterated KH_2PO_4. *Phys. Rev.*, 138:A1539–43, 1965.
3. W. Reese and L. F. May. Studies of phase transitions in order-disorder ferroelectrics. II. Calorimetric investigations of KD_2PO_4. *Phys. Rev.*, 167:504, 1968.
4. W. Reese. Studies of phase transitions in order-disorder ferroelectrics. III. The phase transition in KH_2PO_4 and a comparison with KD_2PO_4. *Phys. Rev.*, 181(2):905–919, 1969.
5. J. W. Benepe and W. Reese. Electronic studies of KH_2PO_4. *Phys. Rev. B*, 3:3032–39, 1971.
6. G. A. Samara. Vanishing of the Ferroelectric and Antiferroelectric states in KH_2PO_4-type crystals at high pressure. *Phys. Rev. Letters*, 27:103–106, 1971.
7. G. A. Samara. The effects of deuteration on the static ferroelectric properties of KH_2PO_4 (KDP). *Ferroelectrics*, 5:25–37, 1973.
8. G. A. Samara. Vanishing of the feroelectricity in displacive and hydrogen-bond ferroelectrics at high pressure. *Ferroelectrics*, 7:221–224, 1974.
9. Blinc R, Burgar M, Čižikov S, Levstik A, Kadaba P, and Shuvalov L A. Dielectric properties of monoclinic KD_2PO_4. *Phys. Stat. Solid. (b)*, 67:689, 1975.
10. S. Endo, T. Sawada, T.Tsukawake, Y. Kobayashi, M. Ishizuka, K. Deguchi, and M. Tokunaga. Vanishing of the ferroelectric state with a finite Currie constant in the hydrogen-bond crystal KD_2PO_4 at high pressure. *Solid State Commun.*, 112:655–660, 1999.
11. Chen R H, Chen-Chieh Yen, Shern C S, and Fukami T. Impedance spectroscopy and dielectric analysis in KH_2PO_4 single crystal. *Solid State Ionics*, 177:2857–2864, 2006.
12. G. E. Bacon and R. S. Pease. A neutron-diffraction study of the ferroelectric transition of potassium dihydrogen phosphate. *Proc. Roy. Soc. A*, 230:359–381, 1955.
13. B. Morosin and G. A. Samara. Pressure effects on the lattice parameters and structure of KH_2PO_4-type crystals. *Ferroelectrics*, 3:49–56, 1971.

14. F.R. Thornley, R.J. Nelmes, and K.D. Rouse. A neutron diffraction study of room-temperature monoclinic KD_2PO4. *Chem. Phys. Letters*, 34:175 – 177, 1975.
15. R. J. Nelmes. The role of crystal-structure determination in the study of structural phase transitions. *Ferroelectrics*, 24:237–245, 1980.
16. R. J. Nelmes, G. M. Meyer, and J. E. Tibballs. The crystal structure of tetragonal KH_2PO_4 and KD_2PO_4 as a function of temperature. *J. Phys. C: Solid State Phys.*, 15:59–75, 1982.
17. J. E. Tibballs, R. J. Nelmes, and G. J. McIntyre. The crystal structure of tetragonal KH_2PO_4 and KD_2PO_4 as a function of temperature and pressure. *J. Phys. C: Solid State Phys.*, 15:37–58, 1982.
18. J. E. Tibballs and R. J. Nelmes. The $P - T$ dependence of the crystal structure of KDP and DKDP above T_c. *J. Phys. C:Solid State Phys.*, 15:L849–L853, 1982.
19. W. F. Kuhs, R. J. Nelmes, and J. E. Tibballs. The proton distribution in KDP above T_c. *J. Phys. C: Solid State Phys.*, 16:L1029–L1032, 1983.
20. R. J. Nelmes. Recent structural studies of the KDP-type transition: A review. *Ferroelectrics*, 53(1-4):207–214, 1984.
21. R. J. Nelmes, W. F. Kuhs, C. J. Howard, J. E. Tibballs, and T. W. Ryan. Structural ordering below T_c in KDP and DKDP. *J. Phys. C: Solid State Phys.*, 18:L711–L716, 1985.
22. Mizuhiko Ichikawa, Kiyosi Motida, and Noboru Yamada. Negative evidence for a proton-tunneling mechanism in the phase transition of KH_2PO_4-type crystals. *Phys. Rev. B*, 36:874–876, 1987.
23. Z. Tun, R. J. Nelmes, W. F. Kuhs, and R. F. D. Stansfield. A high-resolution neutron-diffraction study of the effects of deuteration on the crystal structure of KH_2PO_4. *J. Phys. C: Solid State*, 21:245–258, 1988.
24. R. J. Nelmes. On the structural evidence for a direct proton tunnelling effect in the KH_2PO_4-type transition. *J. Phys. C:Sold State Phys.*, 21:L881–L886, 1988.
25. Satoshi Tanaka. Geometric isotope effect in hydrogen-bonded crystals. *Phys. Rev. B*, 42:10488–98, 1990.
26. M. I. McMahon, R. J. Nelmes, R. O. Piltz, W. F. Kuhs, and N. G. Wright. Neutron-diffraction studies of the heavy-atom structure in H-ordering materials. *Ferroelectrics*, 124:351–354, 1991.
27. J. P. Coignac and H. Poulet. Spectres de vibration du KDP dans les phases para- et ferroélectriques. *Le Journal de Physique*, 32:679–684, 1971.
28. Y. Tominaga, H. Urabe, and M. Tokunaga. Internal modes and local symmetry of PO_4 tetrahedrons in KH_2PO_4 by Raman scattering. *Solid State Commun.*, 48(3):265–267, 1983.
29. H. Furuta, S. Endo, M. Tokunaga, Y. Tominaga, and M. Kobayashi. Local distortion of PO_4 tetrahedra in the paraelectric phase in low temperature under high pressure in KH_2PO_4. *Solid State Commun.*, 117:7–11, 2001.
30. Yasunori Tominaga, Yoshimi Kawahata, and Yuko Amo. Hydrogen modes in KDP/DKDP mixed crystals. *Solid State Commun.*, 125:419–422, 2003.
31. Yoshimi Kawahata and Yasunori Tominaga. Dynamical mechanism of ferroelectric phase transition in KDP/DKDP mixed crystals and distorsion of PO_4 tetrahedron. *Solid State Commun.*, 145:218–222, 2008.
32. I. P. Kaminow and T. C. Damen. Temperature dependence of the ferroelectric mode in KH_2PO_4. *Phys. Rev. Letters*, 20(20):1105–1108, 1968.
33. N. Lagakos and H. Z. Cummings. Preliminary observation of a central peak in the light-scattering spectrum of KH_2PO_4. *Phys. Rev. B*, 10:1063–1069, 1974.
34. P. S. Peercy. Measurements of the "soft" mode and coupled modes in the paraelectric and ferroelectric phases of KH_2PO_4 at high pressure. *Phys. Rev. B*, 12:2725–2740, 1975.
35. Yasunori Tominaga and Hisako Urabe. Central component of $y(xy)x$ Raman spectra in paraelectric KH_2PO_4. *Solid State Commun.*, 41(7):561–564, 1982.
36. J. Watanabe, M. Watanabe, and S. Kinoshita. Stokes-to-anti-Sokes intensity ratio in the low-frequency light scattering of a paraelectric KH_2PO_4 crystal near the ferroelectric phase-transition temperature. *Phys. Rev. B*, 74:132105–4, 2006.
37. J. Watanabe, R. Yoshida, S. Iwane, and S. Kinoshita. Stokes to anti-Stockes intensity ratio in Raman spectra of the soft mode in KH_2PO_4 near the phase transition temperature. *J. Non-Cryst. Solids*, 354:112–116, 2008.
38. S. Yoshioka, Y. Tsujimi, and T. Yagi. A single-exponential time decay of the ferroelectric soft b_2 mode of KDP studied by impulsive stimulated Raman scattering. *Solid State Commun.*, 106:577–580, 1998.
39. Susumu Ikeda, Yukio Noda, Hidehiko Sugimoto, and Yasusada Yamada. Dynamical properties of protons in KH_2PO_4 studied by incoherent neutron scattering. *J. Phys. Soc. Jpn*, 63:1001–1008, 1994.
40. A. V. Belushkin and M. A. Adams. Lattice dynamics of KH_2PO_4 at high pressure. *Physica B*, 234-236:37–39, 1997.
41. G. F. Reiter, J. Mayers, and P. Platzman. Direct observation of tunneling in KDP using neutron Compton scattering. *Phys. Rev. Lett.*, 89(13):135505, Sep 2002.
42. G. Reiter, A. Shukla, P. M. Platzman, and J. Mayers. Deuteron momentum distribution in KD_2PO_4. *New J. Phys.*, 10:013016, 2008.
43. J. C. Slater. Theory of the transition in KH_2PO_4. *J. Chem. Phys.*, 9(1):16–33, 1941.
44. Yutaka Takagi. Theory of the transition in KH_2PO_4, (ii). *J. Phys. Soc. Jpn*, 3:273–274, 1948.
45. Michael E. Senko. Order-disorder model theory for the ferroelectric effect in the dihydrogen phosphates. *Phys. Rev.*, 121:1599–1604, 1961.
46. Henry B Silsbee, Edwin A Uehling, and V Hugo Schmidt. Deuterated intrabond motion and ferroelectricity in KD_2PO_4. *Phys. Rev.*, 133:A165–A170, 1964.
47. F. Y. Wu and Z. R. Yang. The Slater model of $K(H_{1-x}D_x)_2PO_4$ in two dimensions. *J. Phys. C:Solid State Phys.*, 16:L125–L129, 1983.
48. R. Blinc. On the isotopic effects in the ferroelectric behaviour of crystals with short hydrogen bonds. *J. Phys. Chem. Solids*, 13(3-4):204–211, 1960.
49. M. C. Lawrence and G. N. Robertson. The temperature and pressure dependence of the proton tunnelling frequency in KDP. *J. Phys. C: Solid St. Phys.*, 13:L1053–9, 1980.
50. G. N. Robertson and M. C. Lawrence. Analysis of proton tunnelling in KDP using a realistic proton potential. *J. Phys. C: Solid St. Phys.*, 14:4559–4574, 1981.

51. J Skalyo Jr, B C Fraser, and G Shirane. Ferroelectric-mode motion in KD_2PO_4. *Phys. Rev. B*, 1:278–286, 1970.
52. Mizuhiko Ichikawa. O—H vs O···O distance correlation, geometric isotope effect in OHO bonds, and its application to symmetric bonds. *Acta Cryst. B*, 34:2074–2080, 1978.
53. Mizuhiko Ichikawa. Correlation between two isotope effects in hydrogen-bonded crystals. Transition temperature and separation of two equilibrium sites. *Chem. Phys. letters*, 79:583–7, 1981.
54. Eiko Matsushita and Takeo Matsubara. Note on isotope effect in hydrogen bonded crystals. *Prog. Theoret. Phys.*, 67:1, 1982.
55. Shoichi Endo, Toyji Chino, Shinji Tsuboi, and Kichiro Koto. Pressure-induced transition of the hydrogen bond in the ferroelectric compounds KH_2PO_4 and KD_2PO_4. *Nature*, 340:452–455, 1989.
56. Andrzej Katrusiak. Geometric effects of H-atom disordering in hydrogen-bonded ferroelectrics. *Phys. Rev. B*, 48:2992–3002, 1993.
57. Mizuhiko Ichikawa, P. Amasaki, T. Gustafsson, and I. Olovsson. Structural parameters determining the transition temperature of tetragonal KH_2PO_4-type crystals. *Phys. Rev. B*, 64(10):100101, Aug 2001.
58. Kenji K. Kobayashi. Dynamical theory of the phase transition in KH_2PO_4-type ferroelectric crystals. *J. Phys. Soc. Japan*, 24:497–508, 1968.
59. R. Blinc and B. Žekš. Proton-lattice interactions and the soft mode in KH_2PO_4. *J. Phys. C: Solid State Phys.*, 15:4661–4670, 1982.
60. Hidehiko Sugimoto and Susumu Ikeda. Isotope effects in hydrogen-bonded crystal KH_2PO_4. *Phys. Rev. Letters*, 67(10):1306–1309, 1991.
61. Hidehiko Sugimoto and Susumu Ikeda. Electric dipole waves and vibration motion of protons in hydrogen-bonded crystalline KH_2PO_4 at low temperatures. *J. Phys.:CM*, 6:5561–5575, 1994.
62. Yasusada Yamada and Susumu Ikeda. Dynamical properties of protons in KH_2PO_4. I. Proton self-trapped state and its incoherent tunneling. *J. Phys. Soc. Jpn*, 63:3691–3703, 1994.
63. Hidehiko Sugimoto and Susumu Ikeda. Proton transfer in hydrogen-bonded crystalline KH_2PO_4. *J. Phys.:CM*, 8:603–618, 1996.
64. Dalibor Merunka and Boris Rakvin. Molecular dynamics simulation of the soft mode for hydrogen-bonded ferroelectrics. *Phys. Rev. B*, 66:174101, 2002.
65. A. Bussmann-Holder and H. Büttner. Isotope effect on displacive-type ferroelectric-phase-transition temperatures. *Phys. Rev. B*, 41(13):9581–9584, 1990.
66. A. Bussmann-Holder and K. H. Michel. Bond geometry and phase transition mechanism of H-bonded ferroelectrics. *Phys. Rev. Lett.*, 80(10):2173–2176, Mar 1998.
67. Qing Zhang, F. Chen, Nicholas Kioussis, S. G. Demos, and H. B. Radousky. Ab initio study of the electronic and structural properties of the ferroelectric transition in KH_2PO_4. *Phys. Rev. B*, 65(2):024108, Dec 2001.
68. Qing Zhang, Nicholas Kioussis, S. G. Demos, and H. B. Radousky. New evidence of the displacive feature of the ferroelectric transition in KDP -type crystals. *J. Phys.: Condens. Matter*, 14:L89–L93, 2002.
69. S. Koval, J. Kohanoff, R. L. Migoni, and E. Tosatti. Ferroelectricity and isotope effects in hydrogen-bonded KDP crystals. *Phys. Rev. Lett.*, 89(18):187602, Oct 2002.
70. S. Koval, J. Kohanoff, J. Lasave, G. Colizzi, and R. L. Migoni. First-principles study of ferroelectricity and isotope effects in H-bonded KH_2PO_4 crystals. *Physical Review B (Condensed Matter and Materials Physics)*, 71(18):184102, 2005.
71. J. Lasave, S. Koval, N. S. Dalal, and R. Migoni. Slater and takagi defects in KH_2PO_4 from first principles. *Physical Review B (Condensed Matter and Materials Physics)*, 72(10):104104, 2005.
72. S. Ikeda and F. Fillaux. Incoherent-elastic-neutron scattering study of the vibrational dynamics and spin-related symmetry of protons in the $KHCO_3$ crystal. *Phys. Rev. B*, 59:4134–4145, 1999.
73. François Fillaux, Alain Cousson, and David A. Keen. Observation of the dynamical strucuture arising from spatially extended quantum entanglement and long-lived quantum coherence in the $KHCO_3$ crystal. *Phys. Rev. B*, 67:054301 and 189901(E), 2003.
74. François Fillaux, Alain Cousson, and Matthias J. Gutmann. Macroscopic quantum entanglement and "superrigidity" of protons in the $KHCO_3$ crystal from 30 to 300 K. *J. Phys.: Cond. Matter*, 18:3229–3249, 2006.
75. François Fillaux, Alain Cousson, and Matthias J. Gutmann. A neutron diffraction study of macroscopically entangled proton states in the high temperature phase of the $KHCO_3$ crystal at 340 K. *J. Phys.: Cond. Matter*, 20:015225, 2008.
76. François Fillaux, Alain Cousson, and Matthias J. Gutmann. Evidence of macroscopically entangled protons in a mixed crystal of $KH_pD_{1-p}CO_3$. *J. Phys.: Cond. Matter*, 22:045402, 2010.
77. F. Fillaux, M.-H. Limage, and F. Romain. Quantum proton transfer and interconversion in the benzoic acid crystal: vibrational spectra, mechanism and theory. *Chem. Phys.*, 276:181–210, 2002.
78. François Fillaux, François Romain, Marie-Hélène Limage, and Nadine Leygue. Extended tunnelling states in the benzoic acid crystal: Infrared and raman spectra of the OH and OD stretching modes. *Phys. Chem. Chem. Phys.*, 8:4327 – 4336, 2006.
79. François Fillaux and Alain Cousson. Nonlocal protons and deuterons opposed to disorder: a single-crystal neutron diffraction study of $KH_{0.76}D_{0.24}CO_3$ and a theoretical framework. *J. Phys.: Condens. Matter*, 20:252202, 2008.
80. François Fillaux and Alain Cousson. Neutron scattering studies of $K_3H(SO_4)_2$ and $K_3D(SO_4)_2$: The particle-in-a box model for the quantum phase transition. *J. Chem. Phys.*, 137:074504–10, 2012.
81. http://www-llb.cea.fr.
82. D. J. Watkin, C. K. Prout, J. R. Carruthers, P. W. Betteridge, and R. I. Cooper. CRYSTALS. issue 11. Technical report, Chemical Crystallography Laboratory, University of Oxford, England, 1996.
83. See supplementary material at [] for crystallographic information files.
84. See supplementary material Tables at [] for the refined structural parameters.
85. S. W. Lovesey. *Nuclear scattering, Theory of Neutron Scattered from Condensed Matter*, volume I. Clarendon Press, Oxford, 1984.
86. Victoria M. Nield and David A Keen. *Diffuse neutron scattering from crystalline materials*, volume 14 of *Oxford*

series on neutron scattering in condensed matter. Clarendon Press, Oxford, 2001.

87. E. Joos and H. D. Zeh. The emergence of classical properties through interaction with the environment. *Z. Phys. B-Cond. Matter*, 59:223–243, 1985.
88. Wojciech Hubert Zurek. Decoherence and the transition from quantum to classical. *Phys. Today*, 44:36–44, 1991.
89. W. H. Zurek. Decoherence, einselection and the quantum origin of the classical. *Rev. Modern Phys.*, 75(3):715–775, 2003.
90. Piers Coleman. Time crystals. *Nature*, 493:166–167, 2013.
91. M S Schur. Group-theoretical analysis and basis vectors of normal long-wave vibrations of crystals with the KH_2PO_4 structure above their curie point. *Soviet Physics - Crystallography*, 11:394–397, 1966.
92. M S Schur. Group-theoretical analysis and basis vectors of the long wavelength normal vibrations of crystals with the KH_2PO_4 structure below the curie point. *Soviet Physics - Crystallography*, 12:181–185, 1967.
93. Marc Bée. *Quasielastic neutron scattering: principle and applications in solid state chemistry, biology and materials sciences*. Adam Hilger, Bristol and Philadelphia, 1988.
94. S. Haussühl. Anomalous elastic behaviour of monoclinic potassium hydrogen carbonate, $KHCO_3$, in the vicinity of the phase transition at 318 k. *Solid State Comm.*, 57(8):643–647, 1986.
95. François Fillaux. Calculation of infrared and raman band profiles of strong hydrogen bonds. OH stretching band and proton dynamics in crystalline potassium hydrogen carbonate. *Chem. Phys.*, 74:405–412, 1983.
96. F. Fillaux and J. Tomkinson. Proton transfer dynamics in the hydrogen bond. inelastic neutron scattering spectra of na, rb and cs hydrogen carbonates at low temperature. *J. Mol. Struct.*, 270:339, 1992.
97. François Fillaux. Proton transfer in the $KHCO_3$ and benzoic acid crystals: A quantum view. *J. Mol. Struct.*, 844-845:308–318, 2007.
98. G. Eckold, H. Grimm, and M. Stein-Arsic. Proton disorder and phase transition in $KHCO_3$. *Physica B*, 180-181:336–338, 1992.
99. François Fillaux, Alain Cousson, Juan F. R. Archilla, and John Tomkinson. A neutron scattering study of strong-symmetric hydrogen bonds in potassium and cesium hydrogen bistrifluoroacetates: Determination of the crystal structures and of the single-well potentials for protons. *J. Chem. Phys.*, 128:204502, 2008.
100. F. Fillaux, J. Tomkinson, and J. Penfold. Proton dynamics in the hydrogen bond. The inelastic neutron scattering spectrum of potassium hydrogen carbonate at 5 K. *Chem. Phys.*, 124(3):425–437, 1988.
101. The band centered at 1856 cm^{-1} should be assigned to the "zero-phonon" transition involving a shortening of the O···O bond. This transition is not distinctive of the double-well.

Table 1. Energy-levels for the stretching species of protons in KH_2PO_4 ($m = 1$ amu) and extrapolated for deuterons in KD_2PO_4 ($m = 2$ amu) with the double-well operator $\mathbb{V}(\chi) = (450\pm30)\chi+(23400\pm1400)\chi^2+(7400\pm150)\exp-(110\pm10)\chi^2$. $\mathbb{V}$ and χ are in cm^{-1} and Å units, respectively. The minima are at $\pm(0.180 \pm 0.005)$ Å. $h\nu_t$ is the tunnel splitting extrapolated for the symmetrical double-well. The barrier height is (6500 ± 1500) cm^{-1}. Opposite signs for the linear term (the asymmetry parameter) correspond to antiparallel polarizations with respect to the c axis. The eigenstates were computed with a basis-set of 40 harmonic wavefunctions [99].

m (amu)		$h\nu_1$ (cm^{-1})	$h\nu_2$ (cm^{-1})	$h\nu_3$ (cm^{-1})	$h\nu_t$ (cm^{-1})	$h\nu_{0\pm}$ (cm^{-1})
1	Obs.	224 ± 16	2400 ± 100	2680 ± 100	$--$	80 ± 16
	Calc.	224	$2380 - 2300$	$2700 - 2780$	$45 - 138$	$--$
2	Obs.	$--$	1760 ± 100	1960 ± 100	$--$	$--$
	Calc.*	202	1770	2035	13	$--$

*with the preferred operator presented in fig. 5

Table 2. Energy levels for Bloch-states corresponding to parallel ($\Uparrow$) or antiparallel ($\Downarrow$) polarizations with respect to the c-axis of the ferroelectric KH_2PO_4.

$n = \frac{E}{h\nu_1}$	$\lvert n_{1\Uparrow}, n_{2\Uparrow}, n_{3\Uparrow}, n_{4\Uparrow}\rangle$	$\lvert n_{1\Downarrow}, n_{2\Downarrow}, n_{3\Downarrow}, n_{4\Downarrow}\rangle$
8		$\lvert 1_\Downarrow, 1_\Downarrow, 1\Downarrow, 1_\Downarrow\rangle$
7		$\lvert 1_\Downarrow, 1_\Downarrow, 1_\Downarrow, 0_\Downarrow\rangle$; $\lvert 1_\Downarrow, 1_\Downarrow, 0_\Downarrow, 1_\Downarrow\rangle$; $\lvert 1_\Downarrow, 0_\Downarrow, 1_\Downarrow, 1_\Downarrow\rangle$; $\lvert 0_\Downarrow, 1_\Downarrow, 1_\Downarrow, 1_\Downarrow\rangle$
6		$\lvert 1_\Downarrow, 1_\Downarrow, 0_\Downarrow, 0_\Downarrow\rangle$; $\lvert 1_\Downarrow, 0_\Downarrow, 1_\Downarrow, 0_\Downarrow\rangle$; $\lvert 1_\Downarrow, 0_\Downarrow, 0_\Downarrow, 1_\Downarrow\rangle$; $\lvert 0_\Downarrow, 1_\Downarrow, 1_\Downarrow, 0_\Downarrow\rangle$; $\lvert 0_\Downarrow, 1_\Downarrow, 0_\Downarrow, 1_\Downarrow\rangle$; $\lvert 0_\Downarrow, 0_\Downarrow, 1_\Downarrow, 1_\Downarrow\rangle$
5		$\lvert 1_\Downarrow, 0_\Downarrow, 0_\Downarrow, 0_\Downarrow\rangle$; $\lvert 0_\Downarrow, 1_\Downarrow, 0_\Downarrow, 0_\Downarrow\rangle$; $\lvert 0_\Downarrow, 0_\Downarrow, 1_\Downarrow, 0_\Downarrow\rangle$; $\lvert 0_\Downarrow, 0_\Downarrow, 0_\Downarrow, 1_\Downarrow\rangle$
4	$\lvert 1_\Uparrow, 1_\Uparrow, 1_\Uparrow, 1_\Uparrow\rangle$	$\lvert 0_\Downarrow, 0_\Downarrow, 0_\Downarrow, 0_\Downarrow\rangle$
3	$\lvert 1_\Uparrow, 1_\Uparrow, 1_\Uparrow, 0_\Uparrow\rangle$; $\lvert 1_\Uparrow, 1_\Uparrow, 0_\Uparrow, 1_\Uparrow\rangle$; $\lvert 1_\Uparrow, 0_\Uparrow, 1_\Uparrow, 1_\Uparrow\rangle$; $\lvert 0_\Uparrow, 1_\Uparrow, 1_\Uparrow, 1_\Uparrow\rangle$	
2	$\lvert 1_\Uparrow, 1_\Uparrow, 0_\Uparrow, 0_\Uparrow\rangle$; $\lvert 1_\Uparrow, 0_\Uparrow, 1_\Uparrow, 0_\Uparrow\rangle$; $1_\Uparrow, 0_\Uparrow, 0_\Uparrow, 1_\Uparrow\rangle$; $\lvert 0_\Uparrow, 1_\Uparrow, 1_\Uparrow, 0_\Uparrow\rangle$; $\lvert 0_\Uparrow, 1_\Uparrow 0_\Uparrow, 1_\Uparrow\rangle$; $\lvert 0_\Uparrow, 0_\Uparrow, 1_\Uparrow, 1_\Uparrow\rangle$	
1	$\lvert 1_\Uparrow, 0_\Uparrow, 0_\Uparrow, 0_\Uparrow\rangle$; $\lvert 0_\Uparrow, 1_\Uparrow, 0_\Uparrow, 0_\Uparrow\rangle$; $\lvert 0_\Uparrow, 0_\Uparrow, 1_\Uparrow, 0_\Uparrow\rangle$; $\lvert 0_\Uparrow, 0_\Uparrow, 0_\Uparrow, 1_\Uparrow\rangle$	
0	$\lvert 0_\Uparrow, 0_\Uparrow, 0_\Uparrow, 0_\Uparrow\rangle$	

Table 3. Comparison of the energy-levels reported by Reiter et al. for KH_2PO_4 [41] with those computed for the double-well $\mathbb{V}(\chi) = 0.194 \times 10^7\chi^2 + 0.145 \times 10^7 \exp(-1.40\chi^2)$. $\mathbb{V}$ and χ are in cm^{-1} and Å units, respectively. The effective mass is 1 amu. The minima are at $\approx \pm0.18$ Å. The barrier height is ≈ 1400 cm^{-1}. The eigenstates were computed with a basis-set of 40 harmonic wavefunctions [99].

	$h\nu_1$ (cm^{-1})	$h\nu_2$ (cm^{-1})	$h\nu_3$ (cm^{-1})
[41]	758	2800	5088
Calc.	753	2827	5088

Table 4. Bloch-states for opposite orientation of the b axis of $KHCO_3$ below T_c.

$n = \frac{E}{h\nu_1}$	$\lvert n_{u+}, n_{g+}\rangle$	$\lvert n_{u-}, n_{g-}\rangle$
2	$\lvert 1_{u+}, 1_{g+}\rangle$	$\lvert 1_{u-}, 1_{g-}\rangle$
1	$\lvert 1_{u+}, 0_{g+}\rangle$; $\lvert 0_{u+}, 1_{g+}\rangle$	$\lvert 1_{u-}, 0_{g-}\rangle$; $\lvert 0_{u-}, 1_{g-}\rangle$
0	$\lvert 0_{u+}, 0_{g+}\rangle$	$\lvert 0_{u-}, 0_{g-}\rangle$